J. Fluid Mech. (2004), *vol.* 502, *pp.* 273–308.
DOI: 10.1017/S0022112003007705 Printed in the United Kingdom

Direct numerical simulation of compressible turbulent channel flow between adiabatic and isothermal walls

By Y. MORINISHI[1], S. TAMANO[1] AND K. NAKABAYASHI[2]

[1]Department of Mechanical Engineering, Nagoya Institute of Technology, Gokiso-cho, Showa-ku, Nagoya-shi, Aichi-ken, 466-8555 Japan

[2]Department of Mechanical Systems Engineering, Aichi University of Technology, Manori, Nishihasama-cho, Gamagori-shi, Aichi-ken, 443-0047 Japan

(Received 27 November 2001 and in revised form 10 October 2003)

In this paper, the effects of adiabatic and isothermal conditions on the statistics in compressible turbulent channel flow are investigated using direct numerical simulation (DNS). DNS of two compressible turbulent channel flows (Cases 1 and 2) are performed using a mixed Fourier Galerkin and B-spline collocation method. Case 1 is compressible turbulent channel flow between isothermal walls, which corresponds to DNS performed by Coleman *et al.* (1995). Case 2 is the flow between adiabatic and isothermal walls. The flow of Case 2 can be a very useful framework for the present objective, since it is the simplest turbulent channel flow with an adiabatic wall and provides ideal information for modelling the compressible turbulent flow near the adiabatic wall. Note that compressible turbulent channel flow between adiabatic walls is not stationary if there is no sink of heat. In Cases 1 and 2, the Mach number based on the bulk velocity and sound speed at the isothermal wall is 1.5, and the Reynolds number based on the bulk density, bulk velocity, channel half-width, and viscosity at the isothermal wall is 3000.

To compare compressible and incompressible turbulent flows, DNS of two incompressible turbulent channel flows with passive scalar transport (Cases A and B) are performed using a mixed Fourier Galerkin and Chebyshev tau method. The wall boundary conditions of Cases A and B correspond to those of Cases 1 and 2, respectively. Case A corresponds to the DNS of Kim & Moin (1989). In Cases A and B, the Reynolds number based on the friction velocity, the channel half-width, and the kinematic viscosity is 150.

The mean velocity and temperature near adiabatic and isothermal walls for compressible turbulent channel flow can be explained using the non-dimensional heat flux and the friction Mach number. It is found that Morkovin's hypothesis is not applicable to the near-wall asymptotic behaviour of the wall-normal turbulence intensity even if the variable property effect is taken into account. The mechanism of the energy transfers among the internal energy, mean and turbulent kinetic energies is investigated, and the difference between the energy transfers near isothermal and adiabatic walls is revealed. Morkovin's hypothesis is not applicable to the correlation coefficient between velocity and temperature fluctuations near the adiabatic wall.

1. Introduction

It is important to clarify the detailed mechanism of wall-bounded compressible turbulent flow for engineering and industrial applications. Since the 1950s, many

experimental studies have provided valuable knowledge about the friction coefficient, the mean velocity profiles and so on (e.g. see Bradshaw 1977; Fernholz & Finley 1977, 1980; Spina, Smits & Robinson 1994; Smits & Dussauge 1996). The compressibility effects are commonly divided into two types: a mean variable property effect due to the variations in mean properties such as density and viscosity, and an effect due to fluctuations of thermodynamic quantities, mean dilatation and its fluctuation. Morkovin (1962) proposed the hypothesis that the compressibility effect was mainly due to the variable property effect and that the turbulence structures of compressible boundary layers were comparable with those of incompressible ones when the variable property effect was taken into account (see Morkovin 1962; Bradshaw 1977; Smits & Dussauge 1996). This hypothesis has long been widely acknowledged to be correct in the study of the wall-bounded compressible turbulent flow, and is referred to as 'Morkovin's hypothesis'. In the analysis of wall-bounded compressible turbulent flow, the Van Driest transformation (see Van Driest 1951; Rotta 1960), which is supported by Morkovin's hypothesis, is well known. A Reynolds analogy which relates the mass transfer to the heat transfer is well known in incompressible turbulent shear flow (see White 1991). Morkovin (1962) also reported that the Reynolds analogy could be applied to the wall-bounded compressible turbulent flow. This concept is referred to as the 'Strong Reynolds Analogy (SRA)'. The SRA is applicable to the adiabatic wall for compressible turbulent flow. Recently, some modified Reynolds analogies applicable to the isothermal wall have been proposed by Gaviglio (1987), Rubesin (1990) and Huang, Coleman & Bradshaw (1995).

Fernholz & Finley (1980) observed in compressible turbulent zero-pressure-gradient boundary layer flows on isothermal and adiabatic walls that the Van Driest transformed velocity profile agreed well with the data of incompressible turbulent flow. On the other hand, Zhang *et al.* (1993) reported that the untransformed velocity profile near the adiabatic wall agreed well with the data of incompressible turbulent flow. Huang & Coleman (1994) pointed out that the Van Driest transformation did not work well for low Reynolds number flow, while it was useful for high Reynolds number flow (see also Fernholz & Finley 1980; Spina *et al.* 1994). In spite of many experimental efforts, the mean velocity profile of wall-bounded compressible flow remains unclear. Other statistics not sufficiently understood, because experimental measurements, such as of thermodynamic state quantities in high-speed flow, are very difficult (see Spina *et al.* 1994; Smits & Dussauge 1996). The mean temperature profile in the wall-normal direction has in practice been often estimated by using the mean velocity in the experimental study.

In the past decade, with the rapid growth of computational resources, direct numerical simulations (DNS) have been performed as an alternative method to investigate the wall-bounded compressible turbulent flow (e.g. Coleman, Kim & Moser 1995; Guarini *et al.* 2000; Maeder, Adams & Kleiser 2001; Morinishi, Tamano & Nakabayashi 2003). DNS of wall-bounded compressible turbulent flow is appealing because it provides three-dimensional and time-dependent data which are very difficult or even impossible to obtain experimentally. However, there is still a scarcity of DNS results despite their engineering importance. Typical are the DNS results of Coleman *et al.* (1995) for turbulent channel flow between isothermal walls, using the DNS algorithm based on the Legendre Galerkin method. And Guarini *et al.* (2000) performed a DNS of the boundary layer flow on an adiabatic wall, using the DNS algorithm based on the B-spline Galerkin method. They reported that the Van Driest transformed velocity agreed well with the data on the wall-bounded incompressible turbulent flow. However, the influence of different wall

boundary conditions (isothermal and adiabatic conditions) on the mean velocity and temperature profiles has not been investigated. Comparison of compressible and incompressible turbulent flows in terms of the temperature field in addition to the velocity field is also very important for accurate understanding of the compressible turbulent flow. However, there have been no studies to date in which the statistics relating to the temperature of compressible turbulent flow are compared to those of incompressible ones.

In terms of turbulence statistics, Coleman *et al.* (1995) and Guarini *et al.* (2000) reported that the variable property effect should be taken into account in the scaling. However, thermodynamic fluctuations such as density and temperature have not been examined. So, Gatski & Sommer (1998) reported that Morkovin's hypothesis was applicable to the near-wall asymptotic behaviour of turbulence statistics not shown in logarithmic coordinates. Huang *et al.* (1995) showed that their modified Reynolds analogy agreed well with the DNS data of Coleman *et al.* (1995) for compressible turbulent channel flow between isothermal walls. Guarini *et al.* (2000) showed that the modified Reynolds analogy proposed by Huang *et al.* (1995) was effective for boundary layer flow on an adiabatic wall. However, the applicability and usefulness for other flows strongly affected by the opposite wall (e.g. the turbulent channel flow between adiabatic and isothermal walls) have not been examined.

A detailed understanding of the energy transfer in wall-bounded compressible turbulent flow requires data on the turbulent kinetic, mean kinetic and internal energy budgets, because the energy is exchanged among them (see Lele 1994; Huang *et al.* 1995). However, fewer DNS data on the energy budgets for wall-bounded compressible turbulent flow are available than on wall-bounded incompressible turbulent flow. Huang *et al.* (1995) investigated the energy transfer near an isothermal wall using the DNS data on compressible turbulent channel flow presented by Coleman *et al.* (1995). Guarini *et al.* (2000) reported that the turbulent kinetic energy budget near an adiabatic wall in compressible turbulent boundary layer flow was almost the same as that of the corresponding wall-bounded incompressible flow. However, the difference and similarity between energy transfers near isothermal and adiabatic walls is still unknown. In addition, compressible and incompressible flows have not been compared.

In order to understand wall-bounded compressible turbulent flow, it is very important to clarify near-wall turbulence structures in addition to mean velocity and temperature profiles, turbulence statistics and energy transfers. Knowledge on the near-wall turbulence structure for incompressible turbulent flow was summarized by Robinson (1991). On the other hand, there have only been a few studies of near-wall turbulence structure for compressible turbulent flow. Coleman *et al.* (1995) reported that streak structures near an isothermal wall became more coherent in the streamwise direction as the Mach number increased. Guo & Adams (1995) performed DNS of a compressible boundary layer flow developing on a laminar adiabatic wall, an adiabatic wall with constant wall temperature, and showed that streak structures near the wall were larger than those of incompressible turbulent flow. Wang & Pletcher (1996) performed a large-eddy simulation (LES) of isothermal channel flow between hot and cold walls for almost zero Mach number, and reported that the cold wall side exhibited stronger coherence of the near-wall streak structure. LES of turbulent channel flow with constant heat flux for almost zero Mach number was also performed by Dailey & Pletcher (1999) who showed that the turbulent structures appeared to be more coherent on the cold wall side and less coherent on the heating wall side. However, why the modification of the near-wall streak structures

occurs is still not understood. In particular, the detailed turbulence structures near an adiabatic wall have not been found so far. It is also uncertain whether or not Morkovin's hypothesis is successful relative to turbulence structures near adiabatic and isothermal walls.

The purpose of the present study is to investigate the detailed mechanisms in wall-bounded compressible turbulent flow. In particular, wall-bounded flow with an adiabatic wall is still not understood in spite of its engineering importance. In order to clarify compressible turbulent flows near isothermal and adiabatic walls, we perform DNS of compressible turbulent channel flow between adiabatic and isothermal walls, which has not been done previously. The present study of compressible turbulent channel flow between adiabatic and isothermal walls is also very important in complementing the studies of Coleman *et al.* (1995) and Guarini *et al.* (2000).

There is still no universal theory for wall-bounded compressible turbulent flow. Consequently, understanding has usually been obtained from comparison with the incompressible case, for instance the Van Driest transformation. Therefore, understanding of wall-bounded incompressible turbulent flow is also very important for the wall-bounded compressible case. We focus on the similarity and difference between compressible and incompressible turbulent channel flows, as well as the effects of different boundary conditions on compressible turbulent flow. To clarify the difference and similarity between compressible and incompressible turbulent channel flows, DNS of incompressible turbulent channel flow with passive scalar transport between adiabatic and isothermal walls is also carried out. This flow is one of three specific situations distinguished by Teitel & Antonia (1993), and it has not been previously studied by DNS. DNS of incompressible turbulent flow between isothermal walls, which corresponds to that of Kim & Moin (1989), is performed for comparison.

The present paper is arranged as follows. The details of the present DNS data are provided in § 2. In § 3, the effects of the different thermal wall boundary conditions on mean velocity and temperature profiles are explained. In § 4, the profiles of turbulence statistics are discussed. In § 5, the turbulent kinetic, mean kinetic and internal energy budgets are calculated and then the mechanism of energy transfer near isothermal and adiabatic walls is investigated. In § 6, the near-wall turbulence structures near adiabatic and isothermal walls are investigated. Key results are summarized and conclusions are given in § 7. The equations governing compressible and incompressible flows are given in the Appendices.

2. DNS details

2.1. *Numerical methods*

For compressible turbulent channel flow, we use the DNS algorithm based on the B-spline collocation method in the wall-normal (x_2) direction and the Fourier Galerkin method in the streamwise and spanwise (x_1–x_3) directions. The eighth-order B-spline, the resolving power of which is comparable to that of the spectral method, is used in this study. In addition, the skew-symmetric form for the convection term is used in the DNS algorithm to maintain numerical stability. The time-advancement scheme is a third-order low-storage Runge–Kutta method. The detailed DNS algorithm was presented in Morinishi *et al.* (2003), and the validity of the present code was proved by comparing our results with those of existing DNS of compressible turbulent channel flow (Coleman *et al.* 1995). For incompressible

turbulent channel flows, the Chebyshev-tau method is used in the wall-normal direction, and the Fourier Galerkin method is used in the streamwise and spanwise directions. The continuity and Navier–Stokes equations are solved by the modified Kleiser–Schumann method (Kleiser & Schumann 1980; Werne 1995). The skew-symmetric form for the convection term is used to achieve a stable numerical simulation. The semi-implicit time-marching algorithm is used where the diffusion term is treated implicitly with the Crank–Nicolson scheme, and the third-order Runge–Kutta scheme is used for all other terms. The validity of the incompressible code was confirmed by comparing our results with those of the DNS of Kim & Moin (1989) and Horiuti (1992) which were carried out using the same spatial discretization method.

2.2. *Numerical conditions*

The non-dimensional parameters for the present simulations of compressible turbulent channel flows (Cases 1 and 2) are the Reynolds number $Re = 3000$, the Mach number $M = 1.5$, the Prandtl number $Pr = \mu c_p/\kappa = 0.72$, and the ratio of specific heats $\gamma = c_p/c_v = 1.4$ (where κ is thermal conductivity, μ is molecular viscosity, c_p is specific heat at constant pressure, and c_v is specific heat at constant volume). The Reynolds number, $Re = \rho_m U_m H/\mu_{iw}$, is based on the bulk density, bulk velocity, channel half-width, and viscosity at the isothermal wall, and the Mach number, $M = U_m/(\gamma R T_{iw})^{1/2}$ (where $R = (\gamma - 1)c_p/\gamma$ is the gas constant), is based on the bulk velocity and sound speed at the isothermal wall. The low Reynolds and Mach numbers do not make the present analysis useless, because our goal is to clarify the difference and similarity between compressible turbulent flows near adiabatic and isothermal walls. The viscosity is given by Sutherland's law (see (A 5)), where $S_1 = 110.4\,\mathrm{K}$ and $T_{iw} = 293.15\,\mathrm{K}$.

The non-dimensional parameters for the present simulations of incompressible turbulent channel flow with passive scalar transport (Cases A and B) are the Reynolds number $Re_\tau = 150$ and the Prandtl number $Pr = 0.72$. The Reynolds number, $Re_\tau = u_\tau H/\nu$, is based on the friction velocity, the channel half-width, and the kinematic viscosity. Note that the Reynolds number Re_τ is given by $Re_\tau = H/\delta_v$ for compressible turbulent flow, where $\delta_v = \mu_w/(\rho_w u_\tau)$, $u_\tau = (\tau_w/\rho_w)^{1/2}$, and τ_w are the viscous length scale, the friction velocity, and the wall shear stress, respectively.

The initial condition for Case 1 is as follows. The mean streamwise velocity is given by superimposing random velocity fluctuations upon the profile based on Spalding's law (see Spalding 1961). The wall-normal and spanwise velocity components are given as random fluctuations with zero mean values. The temperature and density fluctuations are zero, and their mean values are uniform: $\langle \rho \rangle_{x_1-x_3}/\rho_m = 1$ and $\langle T \rangle_{x_1-x_3}/T_{iw} = 1$, where $\langle\ \rangle_{x_1-x_3}$ represents the spatial average over the x_1- and x_3-directions. Note that the Reynolds average over time and the x_1- and x_3-directions is represented by $\langle\ \rangle$. The initial field for Case 2 is a flow field of Case 1. The no-slip wall boundary condition is used for all cases. The Dirichlet or Neumam boundary condition for the density is not imposed; instead the continuity equation is solved at the wall, keeping the bulk density constant in time. The upper and lower walls of Case 1 are isothermal, and their temperatures are the same. The upper and lower walls of Case 2 are adiabatic and isothermal, respectively. The wall boundary conditions of Cases A and B correspond to those of Cases 1 and 2, respectively. The classification of the computational cases corresponding to thermal wall boundary conditions is shown in table 1. Cases 1I, 2I and 2A represent the isothermal wall side of Case 1, the isothermal wall side of Case 2 and the adiabatic wall side of Case 2, respectively.

	Compressible		Incompressible	
Computational cases	Case 1	Case 2	Case A	Case B
Near isothermal wall	Case 1I	Case 2I	Case AI	Case BI
Near adiabatic wall	–	Case 2A	–	Case BA

TABLE 1. Classification of computational cases corresponding to thermal wall boundary conditions.

Case	Re	Re_τ	M	Pr	γ	$L_1 \times L_2 \times L_3$	$N_1 \times N_2 \times N_3$
1	3000	218	1.5	0.72	1.4	$4\pi H \times 2H \times 4\pi H/3$	$120 \times 180 \times 120$
2	3000	$86.4 - 279$	1.5	0.72	1.4	$4\pi H \times 2H \times 4\pi H/3$	$120 \times 240 \times 120$
A	2291	150	—	0.72	—	$4\pi H \times 2H \times 4\pi H/3$	$128 \times 129 \times 128$
B	2291	150	—	0.72	—	$4\pi H \times 2H \times 4\pi H/3$	$128 \times 129 \times 128$
Coleman *et al.*	3000	222	1.5	0.7	1.4	$4\pi H \times 2H \times 4\pi H/3$	$144 \times 119 \times 80$

TABLE 2. Physical and numerical simulation parameters.

Cases AI, BI and BA represent the isothermal wall side of Case A, the isothermal wall side of Case B and the adiabatic wall side of Case B, respectively.

Grid spacing in the periodic directions is uniform for all cases. The wall-normal collocation points are distributed by using a hyperbolic-tangent function for Cases 1 and 2. The wall-normal grid points are given by Gauss–Lobatto points for Cases A and B. The physical and numerical parameters for all cases are given in table 2. (N_1, N_2, N_3) and (L_1, L_2, L_3) are the number of grid points and computational region in the x_1-, x_2- and x_3-directions, respectively. In the table, parameters of Coleman *et al.* (1995) are also presented for comparison.

The grid resolution is evaluated by using not only the Reynolds number based on the viscous length scale, Re_τ, but also the Reynolds number based on the semi-local viscous length scale, $Re_\tau^* = H/\delta_{v*}$, where $\delta_{v*} = \langle\mu\rangle/(\langle\rho\rangle u_{\tau*})$ and $u_{\tau*} = (\tau_w/\langle\rho\rangle)^{1/2}$ are the semi-local viscous length scale and semi-local friction velocity, respectively. Profiles of Re_τ^* are shown in figure 1. The semi-local wall unit $y^* = y/\delta_{v*}$ is used in the figure, instead of the usual wall unit $y^+ = y/\delta_v$. Grid resolution based on wall and local variables for the present simulations is shown in table 3. The velocity field for Cases A and B does not depend on the temperature field, so the resolution of Case B is the same as that of Case A. The resolution of Cases 1 and 2 is comparable with that of Coleman *et al.* (1995) and Guarini *et al.* (2000) for compressible turbulent flow. The resolution of Cases A and B is better than that of Kim & Moin (1989) and Horiuti (1992) for incompressible turbulent flow. The streamwise resolution near the isothermal wall for compressible turbulent flow seems to be lower than that of incompressible turbulent channel flow. However, when local scaling is used, the resolution becomes comparable. One-dimensional energy spectra and two-point correlations were also examined in Morinishi *et al.* (2003), and we confirmed that the present DNS data had sufficient resolution and domain size. However, the spanwise two-point correlation of density at the centre of the channel was relatively high for Case 1, as it was for the simulation of Coleman *et al.* (1995). They argued that this was caused by acoustic resonance and did not affect other statistics. No problems caused by the acoustic effect appear in the present results of Cases 1 and 2 (see the sections below).

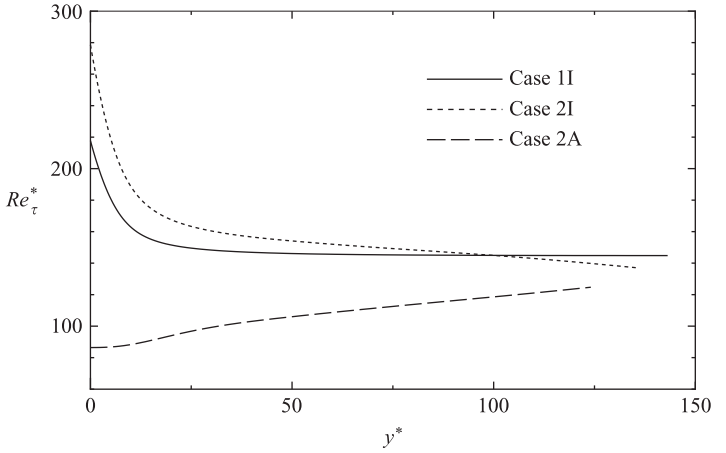

FIGURE 1. Profiles of Reynolds number based on the semi-local viscous length scale.

Case	Δx_1^+	Δx_2^+	Δx_3^+	Δx_1^*	Δx_2^*	Δx_3^*
1I	23	0.36–5.1	7.6	15–23	0.36–3.4	5.1–7.6
2I	29	0.35–4.8	9.7	14–29	0.35–2.4	4.8–9.7
2A	9.1	0.11–1.5	3.0	9.1–13	0.11–2.2	3.0–4.4
A (B)	15	0.045–3.7	4.9	15	0.045–3.7	4.9

TABLE 3. Grid resolution.

3. Mean velocity and temperature profiles

3.1. *Wall laws of mean velocity and temperature*

It is known from dimensional analysis that the mean velocity and temperature profiles depend on the non-dimensional heat flux, $B_q = q_w/(\rho_w c_p u_\tau T_w)$, and the friction Mach number, $M_\tau = u_\tau/(\gamma R T_w)^{1/2}$, when the Prandtl number Pr and the ratio of specific heats γ are constants. Since Pr and γ are fixed in the present simulations, we consider the effects of parameters B_q and M_τ on the mean velocity and temperature profiles. The values of $(-B_q, M_\tau)$ for Cases 1I, 2I and 2A are (0.048, 0.080), (0.059, 0.077) and (0, 0.071), respectively. Parameters B_q and M_τ strongly depend on the mean density as described later, and the variation in the mean density is generally large near the wall in compressible turbulent flow. In this section, the wall laws of the mean velocity and temperature profiles are briefly examined using B_q and M_τ (see Tamano 2002 for details).

Assuming the length scale of turbulence, $l_u = \kappa_u y$, and the temperature length scale, $l_T = \kappa_T y$, the mixing length theory leads to the following equations, respectively (Rotta 1960; Bradshaw 1977):

$$\frac{\mathrm{d}\langle u_1\rangle}{\mathrm{d}y} = \frac{(\tau_w/\langle\rho\rangle)^{1/2}}{\kappa_u y}, \tag{3.1}$$

$$\frac{\mathrm{d}\langle T\rangle}{\mathrm{d}y} = -\frac{\tau_w\langle u_1\rangle + q_w}{\langle\rho\rangle c_p(\tau_w/\langle\rho\rangle)^{1/2}\kappa_T y}. \tag{3.2}$$

The viscous friction work, $\tau_w\langle u_1\rangle$, is induced from the fifth term on the right-hand side of equation (A 3), and it does not appear in incompressible turbulent flow with

passive scalar transport (cf. (B 3) and (A 3)). Equation (3.1) leads to the following equation:

$$\left(\frac{\langle\rho\rangle}{\rho_w}\right)^{1/2}\frac{\mathrm{d}\langle u_1\rangle^+}{\mathrm{d}y^+}=\frac{1}{\kappa_u y^+}, \tag{3.3}$$

where $\langle u_1\rangle^+=\langle u_1\rangle/u_\tau$ is the mean velocity scaled by the friction velocity. The Van Driest transformed velocity $\langle u_1\rangle^+_{VD}$ (see Van Driest 1951) is defined as

$$\langle u_1\rangle^+_{VD}=\int_0^{\langle u_1\rangle^+}(\langle\rho\rangle/\rho_w)^{1/2}\mathrm{d}\langle u_1\rangle^+. \tag{3.4}$$

From (3.3) and (3.4), the log-law of $\langle u_1\rangle^+_{VD}$ is obtained as $\langle u_1\rangle^+_{VD}=\ln y^+/\kappa_u+B$, where B is the additive constant. Assuming $\langle\rho\rangle=\rho_w$, the log-law of $\langle u_1\rangle^+$ is given by $\langle u_1\rangle^+=\ln y^+/\kappa_u+B$. Note that the assumption of $\langle\rho\rangle=\rho_w$ is not correct in the present results.

Next, in order to show the effects of B_q and M_τ on the mean velocities $\langle u_1\rangle^+_{VD}$ and $\langle u_1\rangle^+$ explicitly, we use the relationship between $\langle T\rangle/T_w$ and $\langle u_1\rangle^+$ obtained from (3.1) and (3.2) (see Huang, Bradshaw & Coakley 1994; Huang & Coleman 1994):

$$\langle T\rangle/T_w=1-Pr_t B_q\langle u_1\rangle^+-Pr_t M_\tau^2(\gamma-1)\langle u_1\rangle^{+2}/2, \tag{3.5}$$

where $Pr_t=\kappa_u/\kappa_T$ is the turbulent Prandtl number. Assuming that the pressure given by the state equation (see (A 6)) is constant yields the relationship between density and temperature, $\langle\rho\rangle/\rho_w=T_w/\langle T\rangle$. The relationship between $\langle u_1\rangle^+_{VD}$ and $\langle u_1\rangle^+$ is given by

$$\langle u_1\rangle^+_{VD}=E^{1/2}[\arcsin(A/D+\langle u_1\rangle^+/D)-\arcsin(A/D)], \tag{3.6}$$

where $E=2/[Pr_t M_\tau^2(\gamma-1)]$, $A=B_q/[(\gamma-1)M_\tau^2]$ and $D=(A^2+E)^{1/2}$ (see Huang & Coleman 1994). The rearranged mean velocity in the standard wall-units is given by

$$\langle u_1\rangle^+=D\sin\left[\ln(y^+/y_0^+)\big/\left(\kappa_u E^{1/2}\right)\right], \tag{3.7}$$

where $y_0^+=\exp(-\kappa_u B)$ (see White 1991). In the case of $B_q=M_\tau=0$, the mean velocities $\langle u_1\rangle^+$ and $\langle u_1\rangle^+_{VD}$ are the same as the log-law for incompressible turbulent flow. In the case of $M_\tau=0$, the velocity $\langle u_1\rangle^+$ of (3.7) increases with the increase of $-B_q$, while the transformed velocity $\langle u_1\rangle^+_{VD}$ of (3.6) is independent of $-B_q$. In the case of $B_q=0$, the velocity $\langle u_1\rangle^+$ decreases with the increase of M_τ, while the transformed velocity $\langle u_1\rangle^+_{VD}$ is independent of M_τ.

The mean temperature $\langle T\rangle/T_w$ of (3.5) increases with the increase of $-B_q$ and decreases with the increase of M_τ. The relationship between $\langle T\rangle^+=(T_w-\langle T\rangle)/T_\tau$ and $\langle u_1\rangle^+$,

$$\langle T\rangle^+=Pr_t\langle u_1\rangle^+ + Pr_t M_\tau^2(\gamma-1)\langle u_1\rangle^{+2}/(2B_q), \tag{3.8}$$

is obtained in the case of $B_q\neq 0$ which corresponds to the non-adiabatic wall. The friction temperature T_τ is defined as $T_\tau=B_q T_w$. In the case of $M_\tau=0$, equation (3.8) yields the similarity law of mean velocity and temperature, $\langle T\rangle^+=Pr_t\langle u_1\rangle^+$. The mean temperature $\langle T\rangle^+$ of (3.8) increases with the increase of $-B_q$ and decreases with the increase of M_τ. Note that $\langle T\rangle^+$ depends on B_q even if M_τ is zero, because the mean velocity $\langle u_1\rangle^+$ depends on B_q in the case of $M_\tau=0$. Here, the log-law of the mean temperature near the non-adiabatic wall in compressible turbulent flow depends on the second term on the right-hand side of (3.8) which corresponds to the viscous friction work, and it can usually be neglected in the incompressible case. On the other hand, the log-law of the mean temperature for incompressible turbulent flow

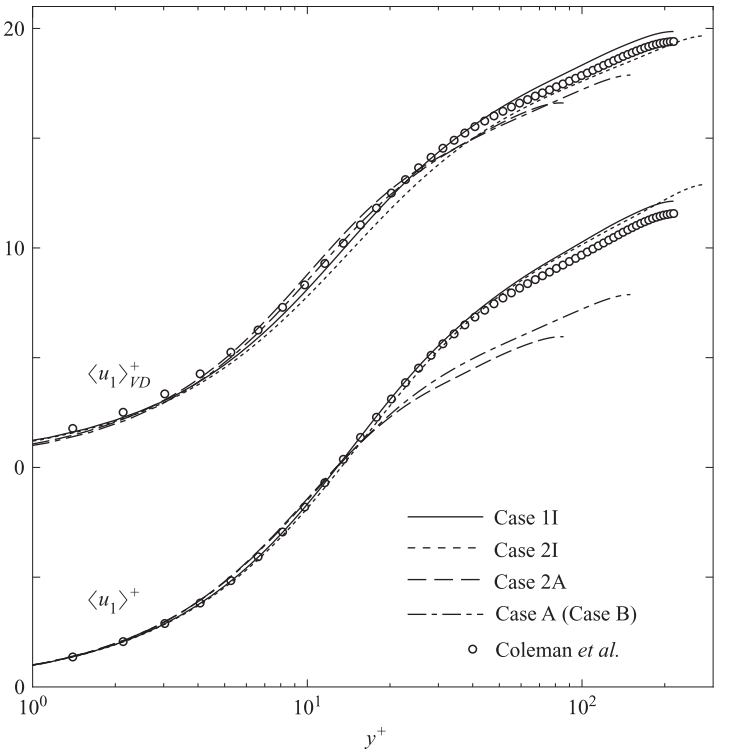

FIGURE 2. Profiles of mean streamwise velocity: $\langle u_1\rangle^+$ and $\langle u_1\rangle^+_{VD}$.

is $\langle T\rangle^+ = (Pr_t/\kappa_u)\ln y^+ + C$, where C is the additive constant (see White 1991). In the following sections, we shall discuss the mean velocity and temperature profiles obtained from the present DNS results, using the analysis in this section.

3.2. *Mean velocity profiles*

Figure 2 shows DNS results for mean velocities $\langle u_1\rangle^+$ and $\langle u_1\rangle^+_{VD}$. The figure shows that the Van Driest transformed velocity $\langle u_1\rangle^+_{VD}$ agrees well with the data of the incompressible turbulent flow. Thus, the Van Driest transformation provides the universal velocity profile, while the standard scaling does not work well because of the failure of the assumption of $\langle\rho\rangle = \rho_w$.

Next, the mean velocities $\langle u_1\rangle^+$ and $\langle u_1\rangle^+_{VD}$ for $y^+ \geqslant 20$, are compared under the same thermal boundary condition. The profiles of mean velocities for Cases 2I and 2A which correspond to compressible turbulent flow near isothermal and adiabatic walls are shown in figure 3. Using the numerical results of figure 3, the effects of the parameters B_q and M_τ on the mean velocity are summarized as follows. The Van Driest transformed velocity $\langle u_1\rangle^+_{VD}$ of Cases 2I and 2A agrees well with the data of Case A, because $\langle u_1\rangle^+_{VD}$ is independent of B_q and M_τ. The velocity $\langle u_1\rangle^+$ of Case 2I is larger than that of Case A because the effect of B_q is larger than that of M_τ. The value of $\langle u_1\rangle^+$ for Case 2A is slightly smaller than that of Case A because of the effect of M_τ. Unlike $\langle u_1\rangle^+$ of Case 2I, $\langle u_1\rangle^+$ of Case 2A is close to that of Case A. This is probably due to the influence of the low-Reynolds-number effect near the adiabatic wall, as mentioned in the Introduction. The profile of $y^+\mathrm{d}\langle u_1\rangle^+/\mathrm{d}y^+$ shows that the log-region of Case 2A is very small (see figure 5*a*).

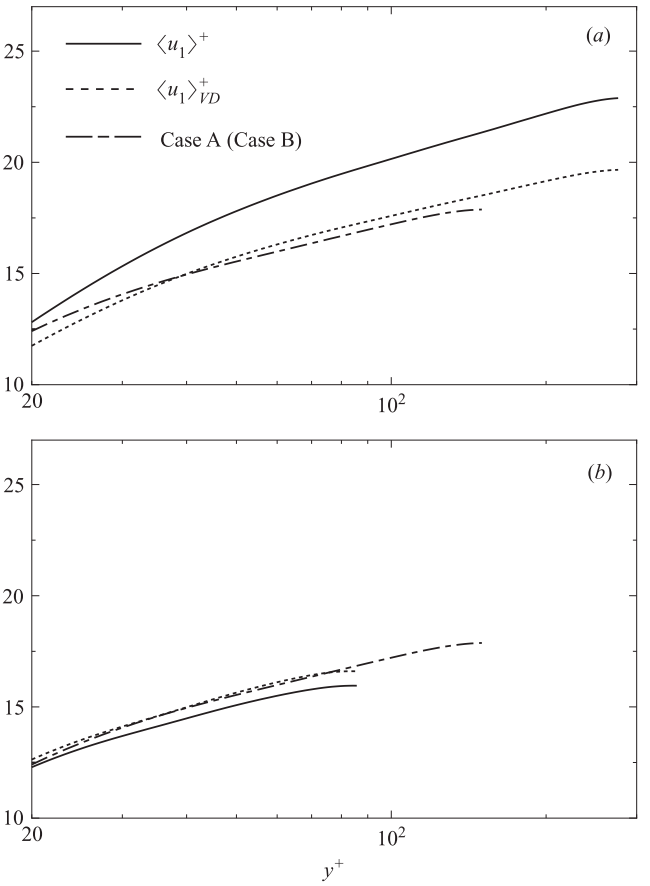

FIGURE 3. Profiles of mean streamwise velocity: (*a*) Case 2I and (*b*) Case 2A.

3.3. *Mean temperature profiles*

DNS results for mean temperature $\langle T \rangle / T_w$ are shown in figure 4(*a*). The temperature $\langle T \rangle / T_w$ for Case 2A becomes smaller than unity, because of the effect of M_τ. The values of $\langle T \rangle / T_w$ for Cases 1I and 2I become larger than unity, because the effect of B_q is larger than that of M_τ. The value of $\langle T \rangle / T_w$ for Case 2I is larger than that of Case 1I because $-B_q$ (=0.048) of Case 1I is smaller than $-B_q$ (=0.059) of Case 2I, and M_τ (=0.080) of Case 1I is larger than M_τ (=0.077) of Case 2I.

Profiles of mean temperature $\langle T \rangle^+$ are given in figure 4(*b*). The temperatures $\langle T \rangle^+$ of compressible turbulent flows (Cases 1I and 2I) are smaller than those of incompressible turbulent flows (Cases AI and BI). The difference in $\langle T \rangle^+$ between Cases 1I and 2I is explained in the same way as for $\langle T \rangle / T_w$. The gradient of $\langle T \rangle^+$ for Cases 2I and BI is large near the centre of the channel, because they are influenced by the opposite wall which corresponds to the adiabatic wall.

Next, to clarify the logarithmic regions of velocity and temperature, the profiles of $y^+ \mathrm{d}\langle u_1 \rangle^+ / \mathrm{d}y^+$ and $y^+ \mathrm{d}\langle T \rangle^+ / \mathrm{d}y^+$ are investigated (see figure 5). The logarithmic regions of the velocity and temperature correspond to the regions where $y^+ \mathrm{d}\langle u_1 \rangle^+ / \mathrm{d}y^+ (= 1/\kappa_u)$ and $y^+ \mathrm{d}\langle T \rangle^+ / \mathrm{d}y^+ (= 1/\kappa_T)$ are constants, respectively. The logarithmic region of velocity appears for all Cases, and the values of $1/\kappa_u$ for Cases 1I and 2I

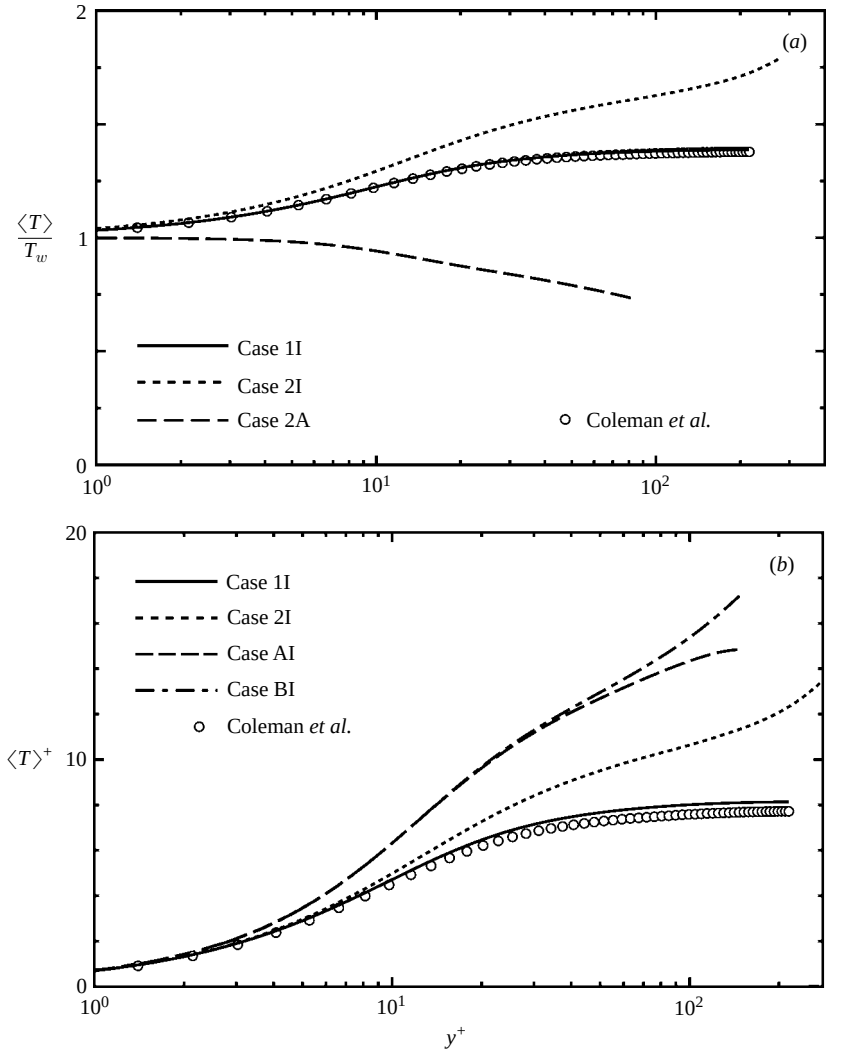

FIGURE 4. Profiles of mean temperature: (*a*) $\langle T\rangle/T_w$ and (*b*) $\langle T\rangle^+$.

are larger those for Cases 2A and A. No logarithmic region of the mean temperature for Case 1I can be seen in figure 5(*b*). Although a plateau region is observed around the minimum point of $y^+\mathrm{d}\langle T\rangle^+/\mathrm{d}y^+$ for Cases 2I and BI, it is caused by the different thermal wall boundary condition on the opposite wall. Since the second term on the right-hand side of (3.8) that corresponds to the viscous friction work is not zero for the compressible turbulent flow, the logarithmic region of temperature is not found for Cases 1I and 2I. The logarithmic region of temperature is also not realized for Case AI in spite of $M_\tau = 0$, because of the low-Reynolds-number effect ($Re_\tau = 150$). The logarithmic region of the mean temperature appears for the incompressible turbulent channel flow with the higher Reynolds number (see Case CI in figure 5*b*). Case CI represents the isothermal wall side of Case C, which has the same conditions as Case A, except the Reynolds number $Re_\tau = 300$, the grid numbers $(N_1, N_2, N_3) = (128, 161, 128)$, and computational region $(L_1, L_2, L_3) = (2\pi H, 2H, 2\pi H/3)$.

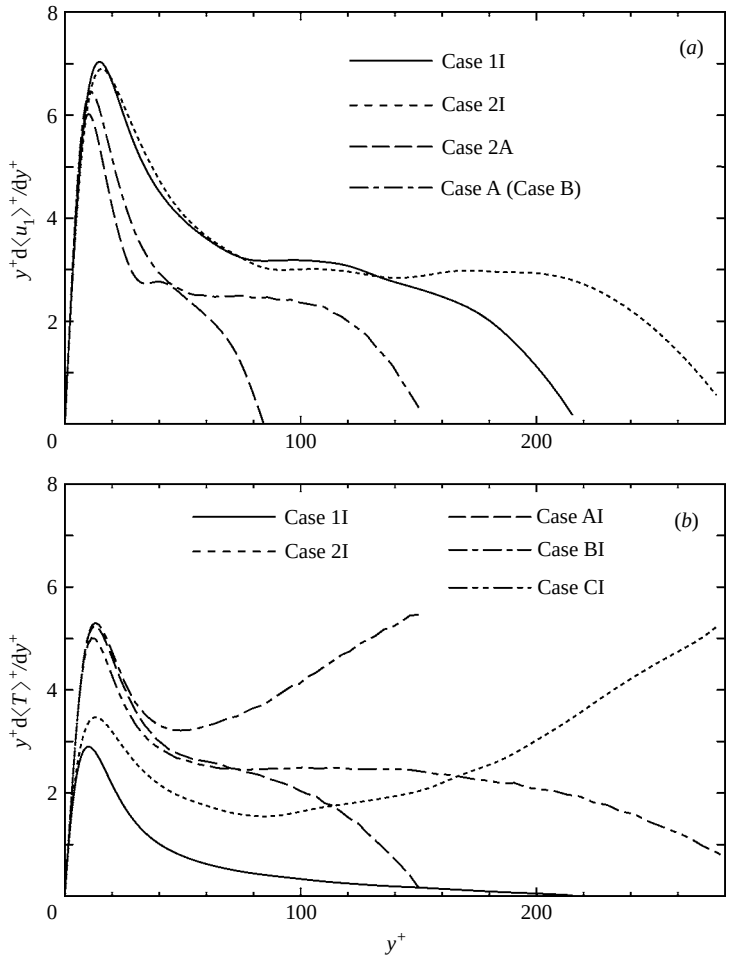

FIGURE 5. Similarity law of mean velocity and temperature: (*a*) $y^+\mathrm{d}\langle u_1\rangle^+/\mathrm{d}y^+$ and (*b*) $y^+\mathrm{d}\langle T\rangle^+/\mathrm{d}y^+$.

4. Turbulence statistics

4.1. *Profiles of turbulence statistics*

The usefulness of the semi-local scaling is investigated by comparing the RMS velocity fluctuations scaled by the friction velocity, $(u'_\alpha)^+_{rms} = \langle u'_\alpha u'_\alpha\rangle^{1/2}/u_\tau$, with those scaled by the semi-local friction velocity, $(u'_\alpha)^*_{rms} = \langle u'_\alpha u'_\alpha\rangle^{1/2}/u_{\tau *}$, ($\alpha = 1, 2, 3$, no summation for α) (see figure 6). The streamwise intensities of turbulence for Cases 1I and 2I in the region $y^+ \geqslant 10$, are larger than those of Case A. The streamwise intensity of turbulence for Case 2A in the region $y^+ \geqslant 10$, is smaller than that of Case A. On the other hand, the semi-local scaling collapses the RMS velocity fluctuations of the compressible turbulent flow onto those of the incompressible one. Namely, Morkovin's hypothesis is satisfied in the RMS velocity fluctuations. However, the wall-normal and spanwise intensities of turbulence, $(u'_2)^*_{rms}$ and $(u'_3)^*_{rms}$, for Case 2A are slightly smaller than those of Case A. The same trend was also observed in the turbulent channel flow with $M = 0$ with variable properties between isothermal walls

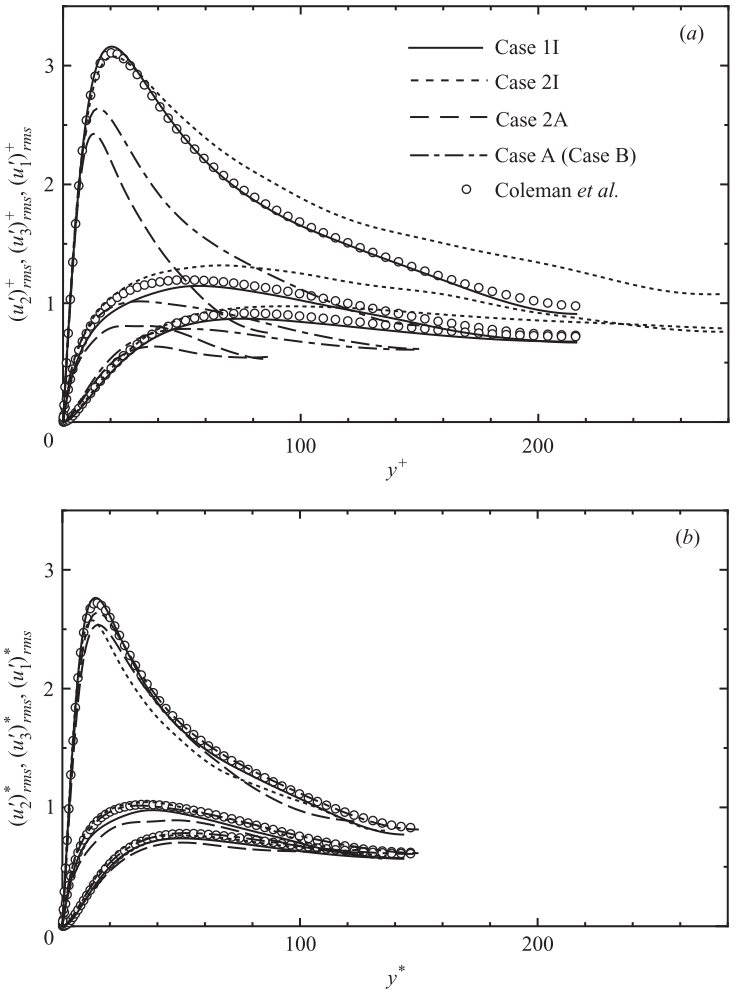

FIGURE 6. Profiles of RMS velocity fluctuations: (*a*) $(u'_\alpha)^+_{rms}$ ($\alpha = 1, 2, 3$) and (*b*) $(u'_\alpha)^*_{rms}$ ($\alpha = 1, 2, 3$).

by Nicoud (1999). The difference may be caused by the low-Reynolds-number effect (see Antonia *et al.* 1992).

The relationship between RMS density and temperature fluctuations has not been investigated to date. The density and temperature fluctuation profiles scaled by the wall and local variables are compared with each other here. The profiles of the RMS density and temperature fluctuations ρ'_{rms}/ρ_w and T'_{rms}/T_w in wall units are shown in figure 7(*a*), and the profiles of $\rho'_{rms}/\langle\rho\rangle$ and $T'_{rms}/\langle T\rangle$ in semi-local wall units are shown in figure 7(*b*). The peak value of ρ'_{rms}/ρ_w for Case 2A is almost twice that of Case 2I, while the peak value of T'_{rms}/T_w for Case 2I is almost twice that of Case 2A. This corresponds to the isobaric change. On the other hand, the RMS temperature fluctuation $T'_{rms}/\langle T\rangle$ is almost the same as the RMS density fluctuation $\rho'_{rms}/\langle\rho\rangle$, except that the RMS temperature fluctuation on the isothermal wall is zero. Further investigation of the appropriate scaling for RMS density and temperature fluctuations is required.

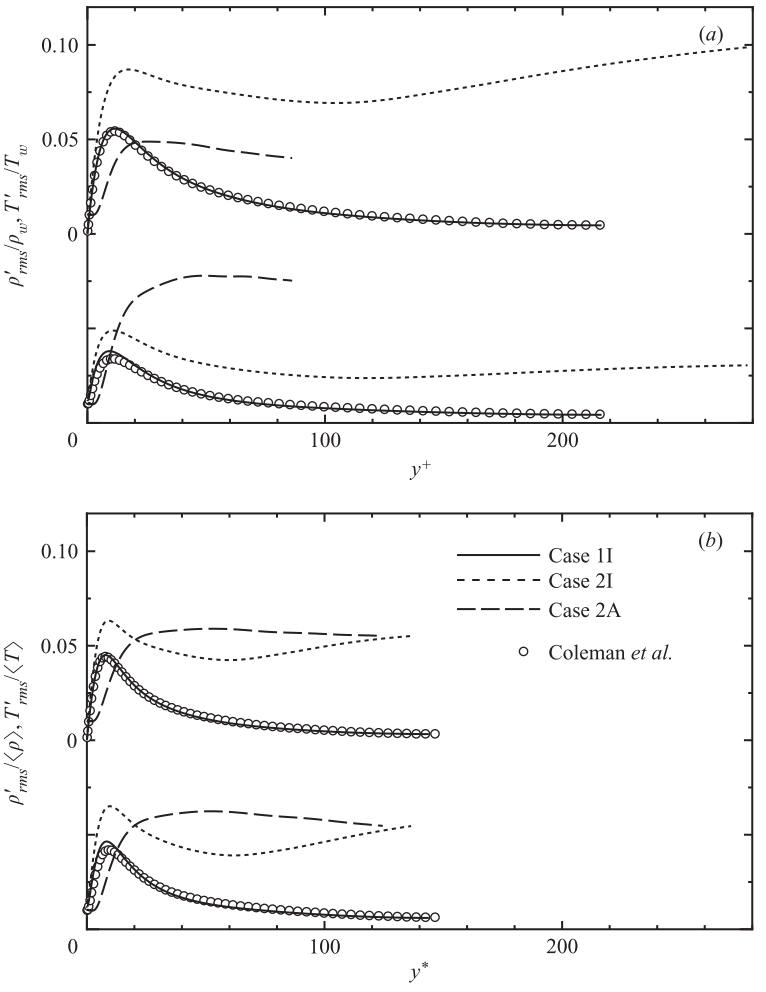

FIGURE 7. Profiles of thermodynamic fluctuations: (*a*) ρ'_{rms}/ρ_w and T'_{rms}/T_w, (*b*) $\rho'_{rms}/\langle\rho\rangle$ and $T'_{rms}/\langle T\rangle$.

Next, we investigate the universal scaling method with respect to the Reynolds shear stress. The Favre average of a quantity ϕ is given by $\{\phi\} = \langle\rho\phi\rangle/\langle\rho\rangle$ and $''$ represents the turbulent fluctuation with respect to the Favre average. The relationships between averaging operations $\langle\,\rangle$ and $\{\,\}$ are as follows:

$$\langle\phi''\rangle = \langle\phi\rangle - \{\phi\}, \tag{4.1}$$

$$\{\phi''\psi''\} = \langle\phi'\psi'\rangle - \langle\phi''\rangle\langle\psi''\rangle + \langle\rho'\phi'\psi'\rangle/\langle\rho\rangle. \tag{4.2}$$

The non-dimensional Reynolds shear stresses are shown in figure 8. The Reynolds shear stresses scaled by the wall variables, $-\langle\rho u'_1u'_2\rangle^+ = -\langle\rho u'_1u'_2\rangle/(\rho_w u_\tau^2)$, $-\langle\rho\rangle\langle u'_1u'_2\rangle^+/\rho_w = -\langle\rho\rangle\langle u'_1u'_2\rangle/(\rho_w u_\tau^2)$ and $-\langle\rho\rangle\{u''_1u''_2\}^+/\rho_w = -\langle\rho\rangle\{u''_1u''_2\}/(\rho_w u_\tau^2)$, have almost the same value, and the Reynolds shear stresses scaled by the local and semi-local variables, $-\langle u'_1u'_2\rangle^* = -\langle\rho\rangle\langle u'_1u'_2\rangle/(\langle\rho\rangle u_{\tau*}^2)$, $-\langle\rho u'_1u'_2\rangle^* = -\langle\rho u'_1u'_2\rangle/(\langle\rho\rangle u_{\tau*}^2)$ and $-\{u''_1u''_2\}^* = -\langle\rho\rangle\{u''_1u''_2\}/(\langle\rho\rangle u_{\tau*}^2)$ coincide with each other. This indicates that the difference in the Reynolds shear stress between Favre and Reynolds averages is negligible. This is because the second and third terms on the right-hand side of

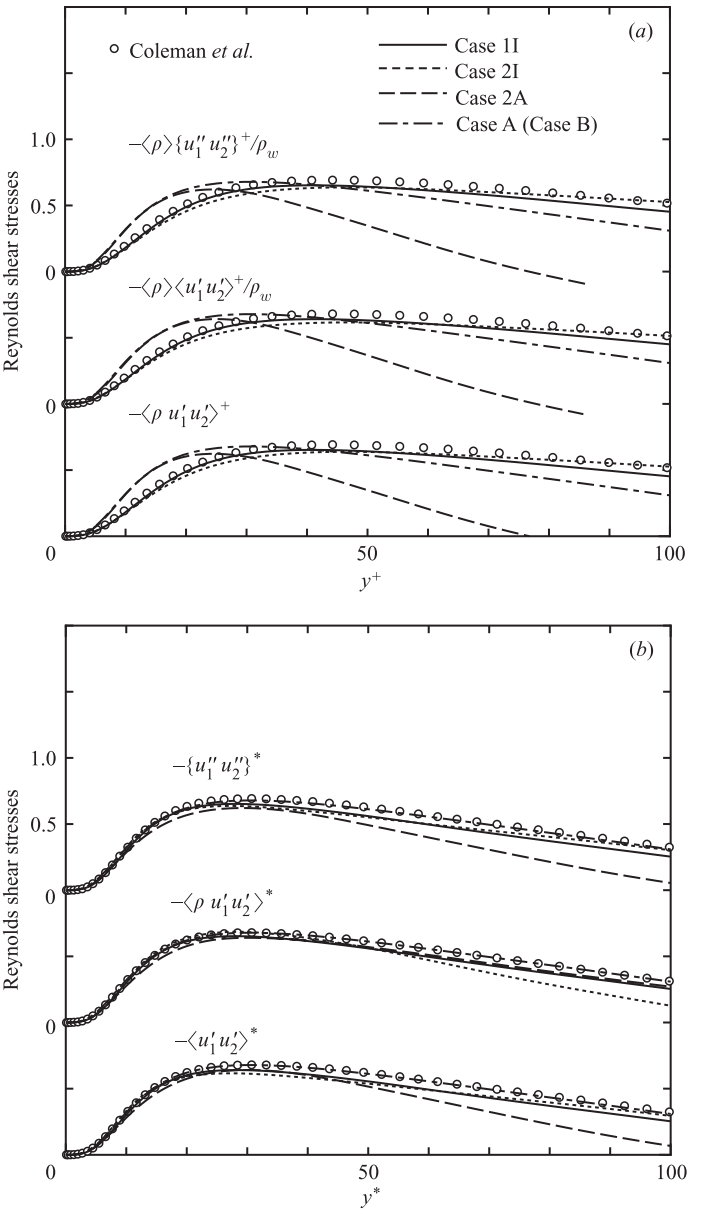

FIGURE 8. Profiles of Reynolds shear stresses.

(4.2) are negligible compared with the first term in the present data. Note that these Reynolds stresses collapse to the same form, provided that the density is constant. The Reynolds shear stresses scaled by the wall variables for Cases 1I and 2I are smaller than that of Case A for $y^+ < 40$ and are almost the same as that of Case A for $y^+ \geqslant 40$. The Reynolds shear stress scaled by the wall variables for Case 2A is almost the same as that of Case A for $y^+ \leqslant 20$ and are smaller than that of Case A for $y^+ > 20$. On the other hand, $-\langle u_1' u_2'\rangle^*$, $-\langle\rho u_1' u_2'\rangle^*$ and $-\{u_1'' u_2''\}^*$ have almost the same value as Case A near adiabatic and isothermal walls. Coleman *et al.* (1995), Guarini *et al.* (2000) and So *et al.* (1998) used $-\langle\rho u_1' u_2'\rangle^+$, $-\langle\rho\rangle\langle u_1' u_2'\rangle^+/\rho_w$

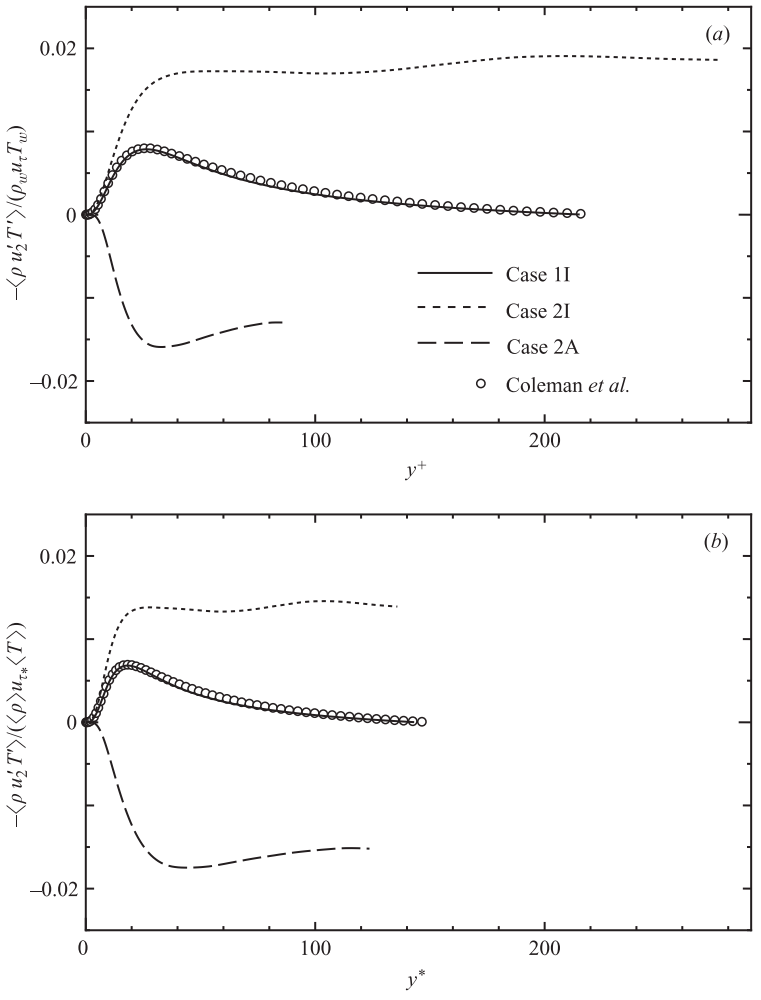

FIGURE 9. Profiles of turbulent heat fluxes.

and $-\langle\rho\rangle\{u_1'' u_2''\}^+/\rho_w$ for the scaling of the Reynolds shear stress, respectively. In the present results, these scaling methods collapse the Reynolds shear stresses onto data for the incompressible turbulent flow (Case A) in the region $y^+ \geqslant 40$ on the isothermal wall side and in the region $y^+ \leqslant 20$ on the adiabatic wall side.

Figure 9 shows the profiles of the turbulent heat flux, $-\langle\rho u_2' T'\rangle/(\rho_w u_\tau T_w)$ and $-\langle\rho u_2' T'\rangle/(\langle\rho\rangle u_{\tau*}\langle T\rangle)$. The sign of the turbulent heat flux of Cases 1I and 2I is opposite to that of Case 2A. Unlike the Reynolds shear stress, the turbulent heat flux does not have a universal profile in the present result, because the turbulent heat flux is directly and strongly influenced by the thermal boundary condition.

4.2. *Near-wall asymptotic behaviour*

4.2.1. *Analytical estimates for near-wall asymptotic behaviour*

The near-wall asymptotic behaviour for Reynolds and Favre averages have been theoretically estimated, when the turbulent fluctuations ϕ' and ϕ'' with respect to Reynolds and Favre averages of ϕ are expanded in terms of y with boundary conditions. Since the density at the wall is governed by the continuity equation, the

Case	$(u_1')_{rms}$	$(u_2')_{rms}$	$(u_3')_{rms}$	$\langle k \rangle$	ε_k	ρ'_{rms}	T'_{rms}	p'_{rms}	$-\langle u_1' u_2' \rangle$	$-\langle u_2' T' \rangle$
1I, 2I	1	1	1	2	0	0	1	0	2	2
2A	1	1	1	2	0	0	0	0	2	1
AI, BI	1	2	1	2	0	–	1	0	3	3
BA	1	2	1	2	0	–	0	0	3	2

TABLE 4. Power index n ($\phi \propto y^n$) of near-wall asymptotic behaviour.

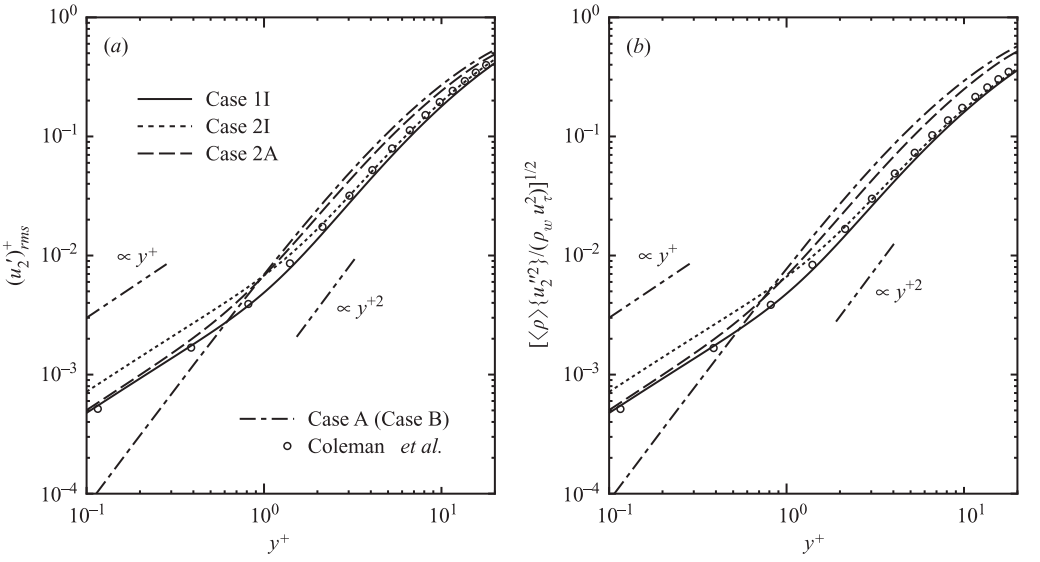

FIGURE 10. Near-wall asymptotic behaviour: (*a*) $(u_2')^+_{rms}$ and (*b*) $[\langle\rho\rangle\{u_2''^2\}/(\rho_w u_\tau^2)]^{1/2}$.

mean density approaches a constant non-zero value with a decrease of y^+ for Cases 1I, 2I and 2A. The continuity equation and the non-slip wall boundary condition provide the relation at the wall, $\partial u_i/\partial x_i|_w = \partial\rho/\partial t|_w/\rho_w$. The density varies in time and space in the present compressible simulations, which yields $\partial u_j/\partial x_j|_w \neq 0$. As a result, $\partial u_2'/\partial x_2|_w$ and $\partial u_2''/\partial x_2|_w$ are not zero for Cases 1 and 2. On the other hand, the continuity equation gives $\partial u_2'/\partial x_2|_w = 0$ for incompressible turbulent flow. Regarding the wall boundary conditions, the near-wall asymptotic behaviour of $(u_\alpha')_{rms}$ ($\alpha = 1, 2, 3$), $\langle k \rangle = \langle u_i' u_i' \rangle/2$, ε_k (see § 5.2), ρ'_{rms}, p'_{rms}, T'_{rms}, $-\langle u_1' u_2' \rangle$ and $-\langle u_2' T' \rangle$ is summarized in table 4. Note that the near-wall asymptotic behaviour of $(u_2')_{rms}$, $-\langle u_1' u_2' \rangle$ and $-\langle u_2' T' \rangle$ for compressible turbulent flow is different from the corresponding incompressible cases.

4.2.2. *Near-wall asymptotic behaviour of turbulence statistics*

The difference in scaling has been investigated for the wall-normal RMS velocities $(u_2')^+_{rms}$ and $[\langle\rho\rangle\{u_2''^2\}/(\rho_w u_\tau^2)]^{1/2}$ (see figure 10). The wall-normal intensities of turbulence, $(u_2')^+_{rms}$, for Cases 1I, 2I and 2A vary linearly with a decrease of y^+, while those of Case A vary linearly with the decrease of y^{+2} as shown in table 4. The near-wall asymptotic behaviour of $[\langle\rho\rangle\{u_2''^2\}/(\rho_w u_\tau^2)]^{1/2}$ is the same as that of $(u_2')^+_{rms}$, where the range of $O(y^{+0})$ near the adiabatic wall is narrower than that near the isothermal wall. This is because the boundary conditions of Favre and Reynolds averages are not different, and the density condition, $\langle\rho\rangle/\rho_w \propto O(y^{+0})$, is

satisfied. On the other hand, So *et al.* (1998), using Morkovin's hypothesis, reported that the near-wall asymptotic behaviour of $[\langle\rho\rangle\{u_2''^2\}/(\rho_w u_\tau^2)]^{1/2}$ became equal to that of the incompressible turbulent flow, because they did not compare the near-wall asymptotic behaviour for compressible and incompressible turbulent flows in logarithmic coordinates. The near-wall asymptotic behaviour of the wall-normal RMS velocity fluctuation for the compressible turbulent flow is not equal to that for the incompressible case, even if the mean density variation is taken into account for the scaling. Thus, Morkovin's hypothesis is not applicable to near-wall asymptotic behaviour.

We confirmed that the near-wall asymptotic behaviour of the other statistics corresponded to the theoretical behaviour in table 4, except for the Reynolds shear stress and turbulent heat flux whose near-wall asymptotic behaviour was not obvious for the compressible turbulent flow because of the small dilatational effect at the wall (see Tamano 2002 for details). The relation between near-wall asymptotic behaviour and the Mach number will be considered in future work.

4.3. *Reynolds analogies*

Morkovin (1962) proposed five SRA relations for the adiabatic wall. One of them is

$$\frac{T'/\langle T\rangle}{(\gamma-1)\langle M\rangle^2 u_1'/\langle u_1\rangle} \approx 1. \tag{4.3}$$

The Reynolds average is used in (4.3) for simplicity. We confirmed that the difference between Favre and Reynolds averages was negligible. Gaviglio (1987), Rubesin (1990) and Huang *et al.* (1995) presented modified Reynolds analogies (GSRA, RSRA and HSRA) which could apply to an isothermal wall. They are given for adiabatic and isothermal walls as follows:

$$\frac{T'/\langle T\rangle}{(\gamma-1)\langle M\rangle^2 u_1'/\langle u_1\rangle} \approx \frac{1}{h(1-g\partial\langle T_t\rangle/\partial\langle T\rangle)}, \tag{4.4}$$

$$\frac{T'/\langle T\rangle}{(\gamma-1)\langle M\rangle^2 u_1'/\langle u_1\rangle} \approx \frac{1}{h(g\partial\langle T_t\rangle/\partial\langle T\rangle-1)}, \tag{4.5}$$

where $T_t = T + u_i^2/(2c_p)$ is a total temperature and $\langle M\rangle = \langle u_1\rangle/\left((\gamma-1)c_p\langle T\rangle\right)^{1/2}$ is a local Mach number. The factors (g, h) of GSRA, RSRA and HSRA are $(1, 1)$, $(1, 1.34)$ and $(1, Pr_t)$, respectively. If (g, h) are $(0, 1)$, the form of (4.4) becomes the same as that of (4.3). GSRA and HSRA are based on the mixing length theory with respect to the streamwise velocity and temperature fluctuations. The turbulent Prandtl number in HSRA is defined as, $Pr_t = \{u_2''u_1''\}\,\partial\{T\}/\partial y/(\{u_2''T''\}\,\partial\{u_1\}/\partial y)$. To examine the applicability and usefulness of the SRA, GSRA, RSRA and HSRA, we introduce a criterion:

$$G \equiv \frac{\langle T'^2\rangle^{1/2}/\langle T\rangle}{(\gamma-1)\langle M\rangle^2\langle u_1'^2\rangle^{1/2}/\langle u_1\rangle}\left(h\left|g\frac{\partial\langle T_t\rangle}{\partial\langle T\rangle}-1\right|\right). \tag{4.6}$$

Note that the root-mean squares $\langle u_1'^2\rangle^{1/2}$ and $\langle T'^2\rangle^{1/2}$ are used instead of u_1' and T'. The model yields the exact value for $G = 1$.

The profiles of G for Cases 1I, 2I and 2A are shown in figure 11, where SRA near the isothermal wall is also considered for comparison. The values of G for SRA are greatly different from unity for Cases 1I and 2I. Although the SRA is satisfied near the adiabatic wall in Guarini *et al.* (2000), the SRA is not successful for Case 2A. The reason is explained below. The SRA is available under the assumption that the total

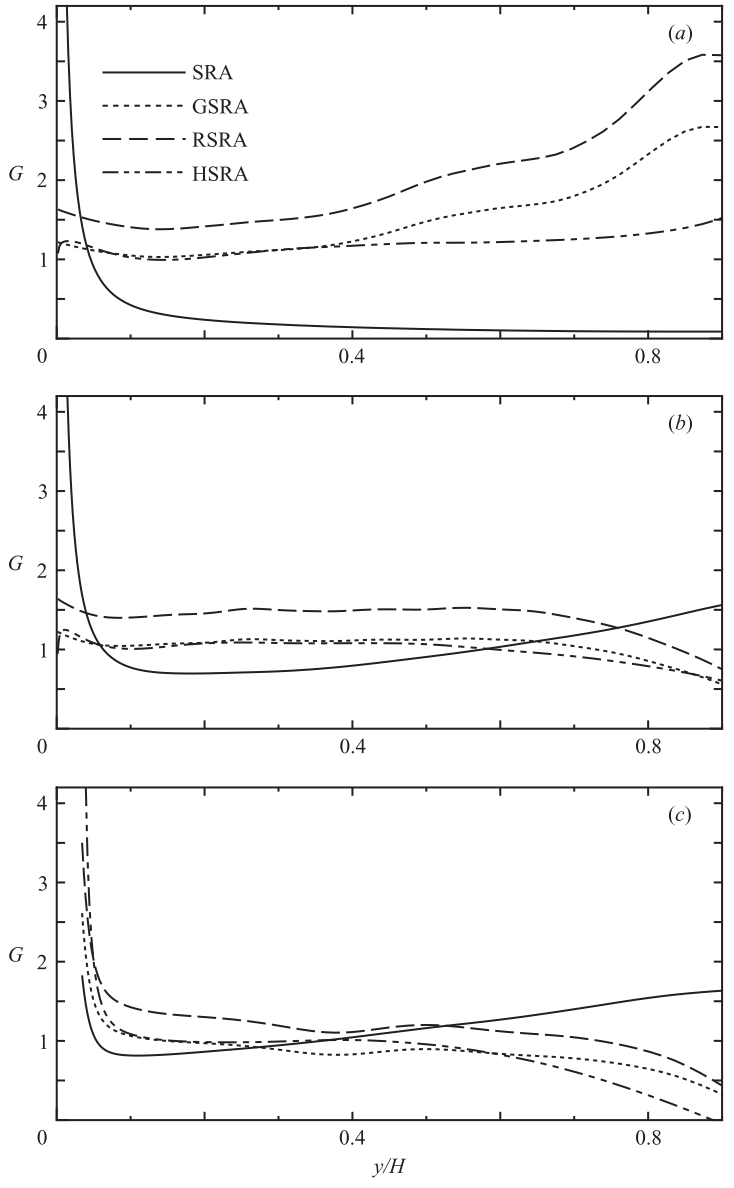

FIGURE 11. Strong Reynolds analogy and modified Reynolds analogies: (*a*) Case 1I, (*b*) Case 2I and (*c*) Case 2A.

temperature fluctuation is negligible compared to the static temperature fluctuation. When the above assumption is not satisfied, the $\langle T'^2\rangle/\langle T\rangle^2 \ll (\langle T_t'^2\rangle - 2\langle T'T_t'\rangle)/\langle T\rangle^2$ condition presented by Guarini *et al.* (2000) must be satisfied. However, we confirmed that both the assumption and condition were not satisfied for Case 2A.

The region of $G \simeq 1$ of HSRA is larger than that of GSRA for Case 1I, because the turbulent Prandtl number is treated as a variable in HSRA and unity in GSRA. The values of G for HSRA and GSRA for Cases 2I and 2A are almost unity in the region $y/H < 0.6$ and decrease gradually in the region $y/H > 0.6$ where the influence of the opposite wall is not negligible. The value of G for RSRA is larger than those

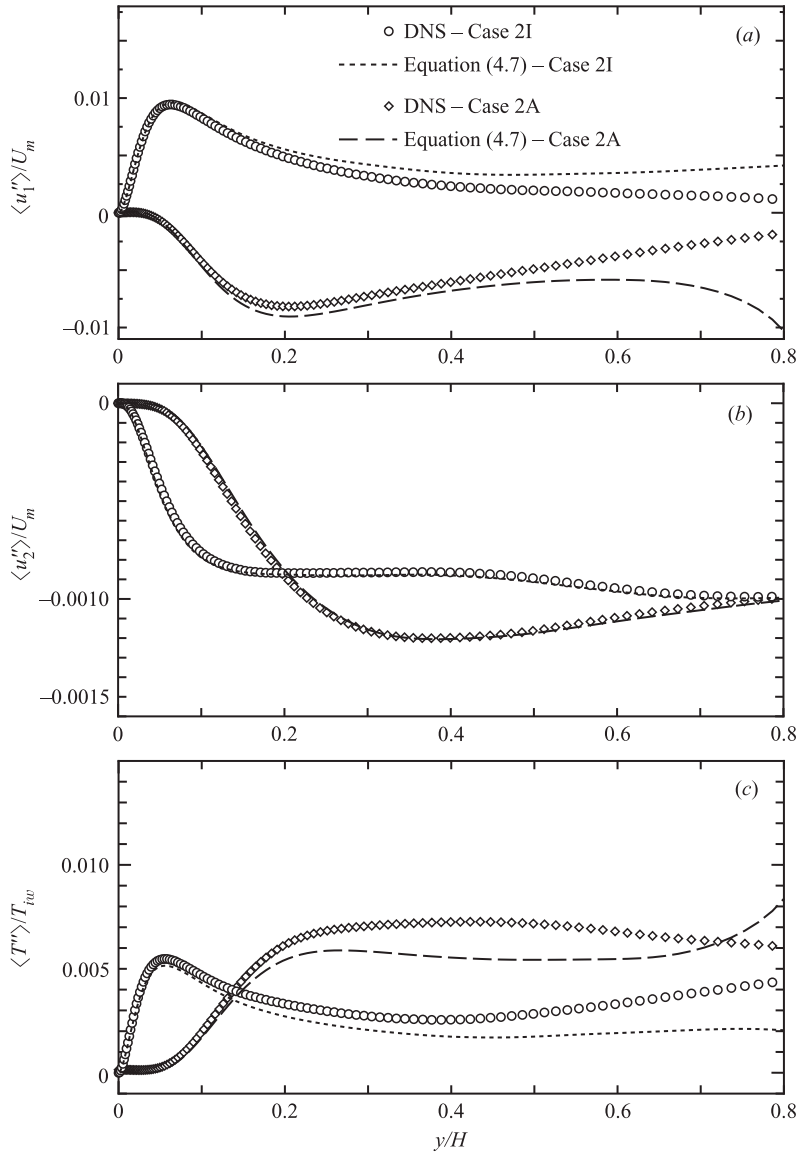

FIGURE 12. Mean Favre-averaged fluctuations: (*a*) $\langle u_1'' \rangle$, (*b*) $\langle u_2'' \rangle$ and (*c*) $\langle T'' \rangle$.

for HSRA and GSRA for all cases. It is found that the existing modified Reynolds analogies do not completely agree with the DNS data on the compressible turbulent flow between adiabatic and isothermal walls.

Huang *et al.* (1995) also proposed the model for mean Favre-averaged fluctuations $\langle \phi'' \rangle$:

$$\langle \phi'' \rangle = \{u_2'' T''\}\{u_1'' \phi''\}/(\{T\}\{u_1'' u_2''\}), \tag{4.7}$$

using a new strong Reynolds analogy. Figure 12 shows comparisons of the present DNS results of Cases 2I and 2A with (4.7) for $\langle u_1'' \rangle$, $\langle u_2'' \rangle$ and $\langle T'' \rangle$. The model of Huang *et al.* almost agrees with the DNS results for $\langle u_1'' \rangle$ in the region $y/H < 0.5$ where the influence of the opposite wall is negligible. The agreement on $\langle u_2'' \rangle$ is very

good. The difference in $\langle T'' \rangle$ between the model and the DNS result for Case 2A is slightly large in the region $y/H > 0.2$.

5. Energy transfers

5.1. *Conservation equations*

The Favre-averaged mean-flow kinetic energy $\{K\}$, the Favre-averaged turbulent kinetic energy $\{k\}$, the Favre-fluctuation mean-flow kinetic energy K'' and the Favre-fluctuation turbulent kinetic energy k'' are defined as $\{K\} \equiv \{u_i\}^2/2$, $\{k\} \equiv \{u_i'' u_i''\}/2$, $K'' \equiv \{u_i\} u_i''$ and $k'' \equiv u_i'' u_i''/2 - \{k\}$, respectively. The continuity, momentum and total energy equations are as follows in fully developed turbulent channel flow (see Huang *et al.* 1995);

$$\frac{\partial \langle \rho \rangle \{u_2\}}{\partial x_2} = 0, \tag{5.1}$$

$$\frac{\partial \langle \rho \rangle \{u_i\}\{u_2\}}{\partial x_2} = \frac{\partial \langle \tau_{i2} \rangle}{\partial x_2} - \frac{\partial \langle \rho \rangle \{u_i'' u_2''\}}{\partial x_2} + \langle \rho \rangle f_i, \tag{5.2}$$

$$\frac{\partial \langle \rho \rangle \{u_2\}[\{K\} + \{k\} + c_v\{T\} + \langle p \rangle / \langle \rho \rangle]}{\partial x_2} = \frac{\partial [\langle \tau_{i2} \rangle \langle u_i \rangle + \langle \tau_{i2}' u_i' \rangle - \langle q_2 \rangle]}{\partial x_2} - \frac{\partial [\langle \rho \rangle \{u_2'' K''\} + \langle \rho \rangle \{u_2'' k''\} + \langle \rho \rangle c_p \{u_2'' T''\}]}{\partial x_2} + \langle \rho \rangle f_1 \{u_1\}, \tag{5.3}$$

where $\{u_2'' K''\} = \{u_2'' u_i''\}\{u_i\}$ and $\{u_2'' k''\} = \{u_2 u_i u_i\}/2 - \{u_2\}\{u_i\}\{u_i\}/2 - \{u_2'' u_i''\}\{u_i\} - \{u_i'' u_i''\}\{u_2\}/2$. The averaged state equation is $\langle p \rangle = (\gamma - 1) c_p \langle \rho \rangle \{T\}/\gamma$. The Reynolds averaged viscous stress tensor $\langle \tau_{ij} \rangle$ is defined as

$$\langle \tau_{ij} \rangle = \langle \mu \rangle \left(\frac{\partial \langle u_i \rangle}{\partial x_j} + \frac{\partial \langle u_j \rangle}{\partial x_i} \right) - \frac{2}{3} \langle \mu \rangle \langle d \rangle \delta_{ij} + \left\langle \mu' \left(\frac{\partial u_i'}{\partial x_j} + \frac{\partial u_j'}{\partial x_i} \right) \right\rangle - \frac{2}{3} \langle \mu' d' \rangle \delta_{ij}, \tag{5.4}$$

where $\langle d \rangle = \partial \langle u_j \rangle / \partial x_j$ and $d' = \partial u_j' / \partial x_j$. The fluctuation viscous stress tensor, $\tau_{ij}' = \tau_{ij} - \langle \tau_{ij} \rangle$, is defined as

$$\tau_{ij}' = \langle \mu \rangle \left(\frac{\partial u_i'}{\partial x_j} + \frac{\partial u_j'}{\partial x_i} \right) - \left\langle \mu' \left(\frac{\partial u_i'}{\partial x_j} + \frac{\partial u_j'}{\partial x_i} \right) \right\rangle - \frac{2}{3} \langle \mu \rangle d' \delta_{ij} + \frac{2}{3} \langle \mu' d' \rangle \delta_{ij} + \mu' \left(\frac{\partial u_i'}{\partial x_j} + \frac{\partial u_j'}{\partial x_i} \right) - \frac{2}{3} \mu' d' \delta_{ij} + \mu' \left(\frac{\partial \langle u_i \rangle}{\partial x_j} + \frac{\partial \langle u_j \rangle}{\partial x_i} \right) - \frac{2}{3} \mu' \langle d \rangle \delta_{ij}. \tag{5.5}$$

The Reynolds-averaged heat flux is given by $\langle q_2 \rangle = -\langle \kappa \rangle \partial \langle T \rangle / \partial x_2 - \langle \kappa' \partial T' / \partial x_2 \rangle$.

The total energy is defined as the sum of the turbulent kinetic energy $\{k\}$, the mean kinetic energy $\{K\}$ and the internal energy, $\{e\} = c_v\{T\}$, and it should be conserved in compressible turbulent channel flow. We confirmed that the conservation of the total energy was satisfied in the present simulations of Cases 1 and 2. On the other hand, there are energy transfers among $\{k\}$, $\{K\}$ and $\{e\}$. In the subsequent sections, we shall clarify the mechanism of energy transfer through these energy budgets.

5.2. *Energy budgets*

The turbulent kinetic energy equation is

$$P_k + D_k - \varepsilon_k + C_k = 0, \tag{5.6}$$

where the production $P_k = -\langle \rho \rangle \{u_1'' u_2''\} \partial \{u_1\} / \partial x_2$, diffusion $D_k = \partial [\langle \tau_{i2}' u_i' \rangle - \langle \rho \rangle \{u_2'' k''\} - \langle p' u_2' \rangle] / \partial x_2$, dissipation per unit volume $\varepsilon_k = \langle \tau_{ij}' \partial u_i' / \partial x_j \rangle$ and compressibility

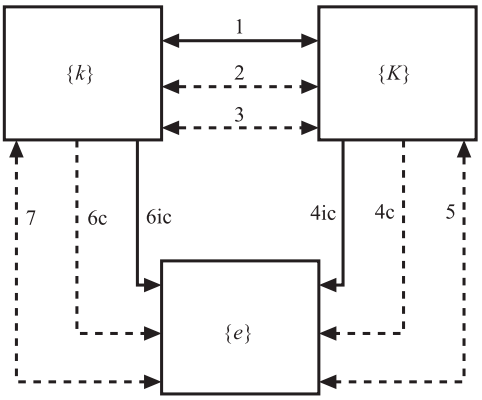

FIGURE 13. Energy transfer of wall-bounded compressible turbulent flow: 1. $P_k(=\varepsilon_{TK})$, 2. C_{k1}, 3. C_{k2}, 4c. ε_{VKc}, 4ic. ε_{VKi}, 5. C_{K1}, 6c. $\langle\rho\rangle\varepsilon_{cc}$, 6ic. $\langle\rho\rangle\varepsilon_{ci}$, 7. C_{k3}. These terms are defined in §§ 5.2 and 5.4. Terms 4c, 4ic, 6c and 6ic are irreversible. Dashed arrows indicate compressibility terms.

term $C_k = -C_{k1} + C_{k2} + C_{k3}$, where $C_{k1} = \langle u_2''\rangle\partial\langle p\rangle/\partial x_2$, $C_{k2} = \langle u_i''\rangle\partial\langle\tau_{i2}\rangle/\partial x_2$ and $C_{k3} = \langle p'\partial u_k'/\partial x_k\rangle$. The mean kinetic energy equation is

$$D_K - \varepsilon_{TK} - \varepsilon_{VK} + C_K + F_K = 0, \tag{5.7}$$

where the diffusion $D_K = \partial[\langle\tau_{i2}\rangle\langle u_i\rangle - \langle\rho\rangle\{u_2''K''\} - \langle p\rangle\langle u_2\rangle]/\partial x_2$, turbulent dissipation per unit volume $\varepsilon_{TK}(=P_k)$, viscous dissipation per unit volume $\varepsilon_{VK} = \langle\tau_{i2}\rangle\partial\langle u_i\rangle/\partial x_2$, compressibility term $C_K = C_{k1} - C_{k2} + C_{K1}$, $C_{K1} = \langle p\rangle\partial\langle u_2\rangle/\partial x_2$, and force term $F_K = \langle\rho\rangle f_1\{u_1\}$. After turbulent kinetic and mean kinetic energy equations are subtracted from the total energy equation (5.3), the internal energy equation is obtained as

$$D_e + \varepsilon_{VK} + \varepsilon_k - C_{K1} - C_{k3} = 0, \tag{5.8}$$

where $D_e = D_{e1} + D_{e2}$ is the diffusion term, $D_{e1} = -\partial\langle\rho\rangle c_v\{u_2''T''\}/\partial x_2$, and $D_{e2} = -\partial\langle q_2\rangle/\partial x_2$. From (5.6), (5.7) and (5.8), the energy transfers among turbulent kinetic, mean kinetic and internal energies are represented as seven terms (see Huang *et al.* 1995). 1. $P_k(=\varepsilon_{TK})$, 2. C_{k1}, 3. C_{k2}, 4. ε_{VK}, 5. C_{K1}, 6. ε_k, 7. C_{k3}. Terms 2, 3, 5 and 7 represent the compressibility terms. Terms 4 and 6 which represent the irreversible energy transfers can be divided into the terms involving fluctuating dilatation or fluctuating viscosity (4c, 6c) and the variable-density extended terms of the pseudo-dissipation used in the incompressible flow (4ic, 6ic), respectively (see § 5.4 for details). Terms 4 and 6 were not divided in the study of Huang *et al.* (1995). Energy transfers for wall-bounded compressible turbulent flow are summarized in figure 13. The dashed arrows represent the compressibility terms.

Turbulent kinetic energy budgets of Cases 1 and 2 are shown in figure 14, in which the profiles are scaled by bulk variables, $\rho_m U_m^3/H$. Here, Huang *et al.* (1995) used a mixture of wall and bulk variables, $\tau_w U_m/H$, and Guarini *et al.* (2000) used wall variables, $\rho_w u_\tau/\delta_v$, for scaling the turbulent kinetic energy budget. The peak value of the production term P_k (term 1 of figure 13) near the adiabatic wall is smaller and its location moves to the centre of the channel, compared with that of P_k near the isothermal wall (see figure 14*b*). The compressibility term in the turbulent kinetic energy equation, C_k, and the turbulent kinetic energy dissipation rate per unit volume, ε_k, are discussed in § 5.3 and § 5.4, respectively.

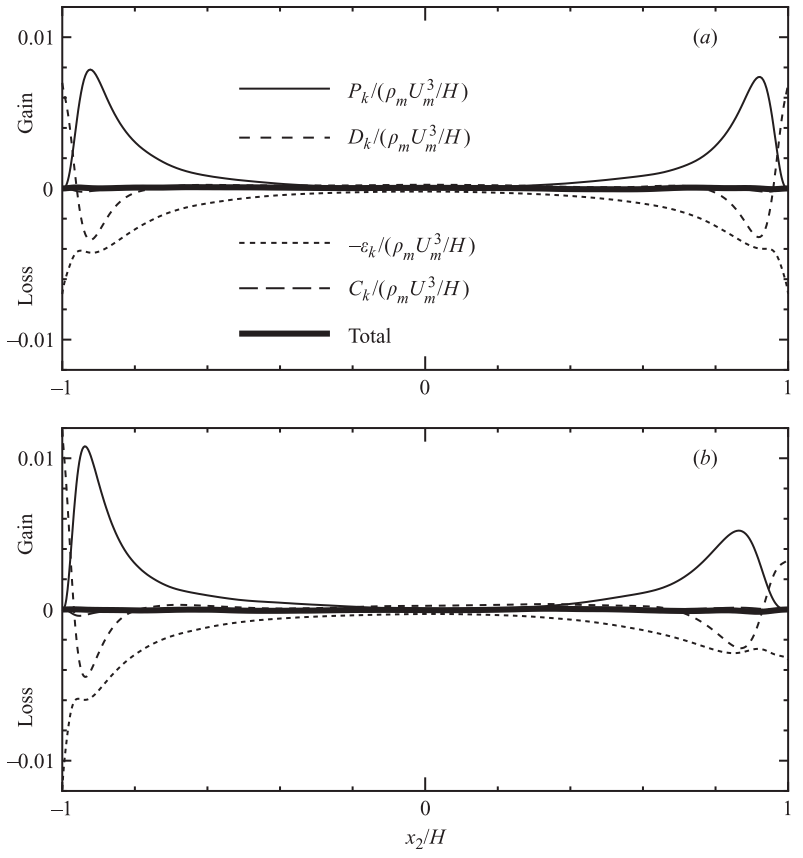

FIGURE 14. Turbulent kinetic energy budgets: (*a*) Case 1 and (*b*) Case 2. The upper and lower walls of Case 1 are isothermal. The upper and lower walls of Case 2 are adiabatic and isothermal, respectively.

Next, we consider the budgets scaled by a mixture of local and semi-local variables, $\langle\rho\rangle u_{\tau*}^3/\delta_{v*}$, for Cases 2I and 2A (see figure 15). Lechner, Sesterhenn & Friedrich (2001) performed DNS of turbulent supersonic isothermal-wall channel flow at the same parameters as Coleman *et al.* (1995) at improved resolution, using the DNS algorithm based on a Padé (compact) finite-difference method, and reported that the production and dissipation rates in the turbulent kinetic energy equation normalized by $\tau_w U_m/H$ were reduced compared to their incompressible counterparts. However, figure 15 shows that the production and dissipation terms of Cases 2I and 2A agree well with the data of Case A. This indicates that the difference observed in the turbulent kinetic energy budget scaled by $\rho_m U_m/H$ or $\tau_w U_m/H$ is mainly due to the variable property effect.

The mean kinetic energy budgets of Cases 1 and 2 are shown in figure 16. We confirmed that the mean kinetic energy budget of Case 1 was not essentially different from that of Case A, and that the difference between budgets near adiabatic and isothermal walls for Case 2 was mainly due to the variable property effect. The compressibility term in the mean kinetic energy equation, C_K, and the viscous dissipation per unit volume, ε_{VK}, are discussed in § 5.3 and § 5.4, respectively.

The internal energy budgets of Cases 1 and 2 are shown in figure 17, and the energy (passive scalar) budgets of Cases A and B are shown in figure 18. For Cases A and

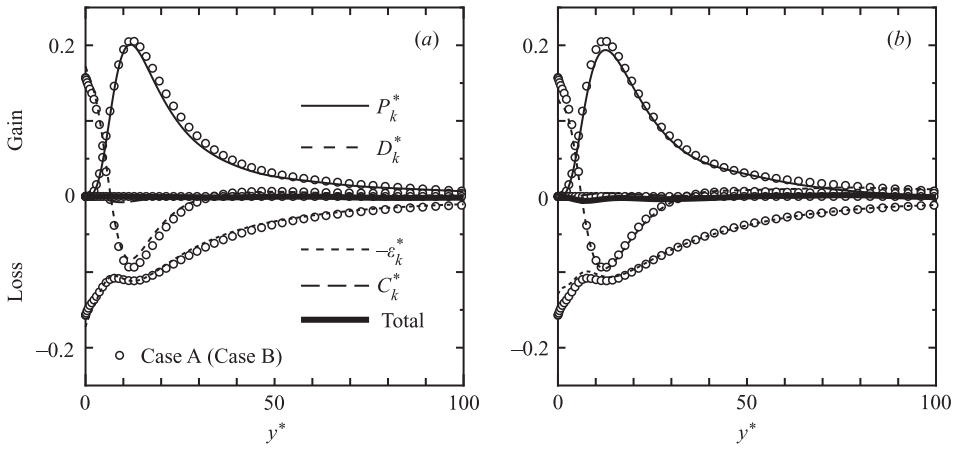

FIGURE 15. Turbulent kinetic energy budgets in semi-local wall units: (*a*) Case 2I and (*b*) Case 2A.

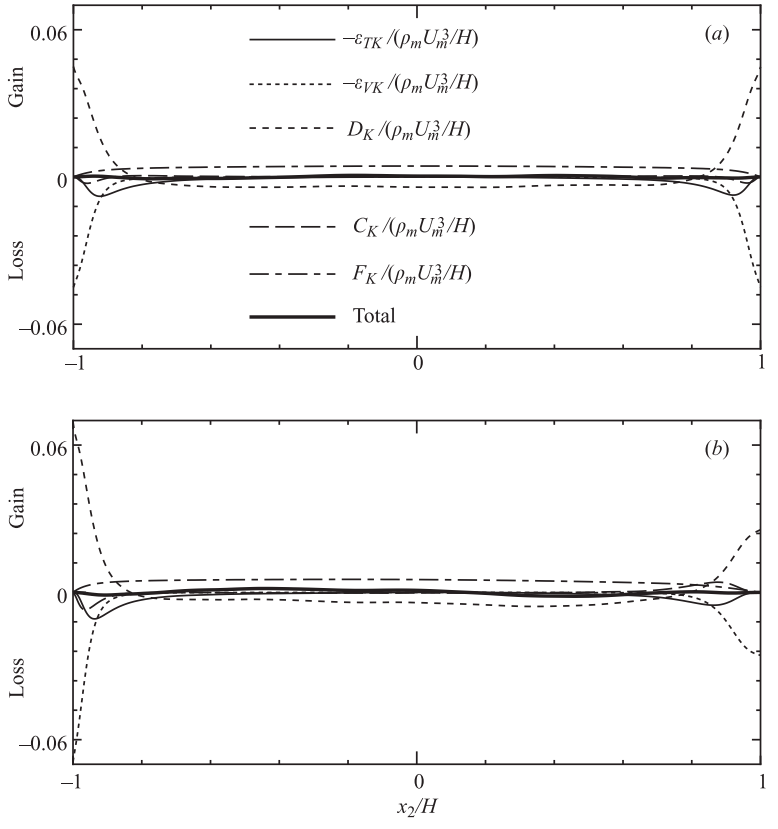

FIGURE 16. Mean kinetic energy budgets: (*a*) Case 1 and (*b*) Case 2.

B, the bulk velocity U_m and the friction temperature T_τ at the isothermal wall are used for scaling the energy budgets. The dissipation rates ε_k and ε_{VK} are irreversible energy transfers from the turbulent kinetic and mean kinetic energies to the internal energy, respectively. On the other hand, the energy transfer due to the dissipation rate

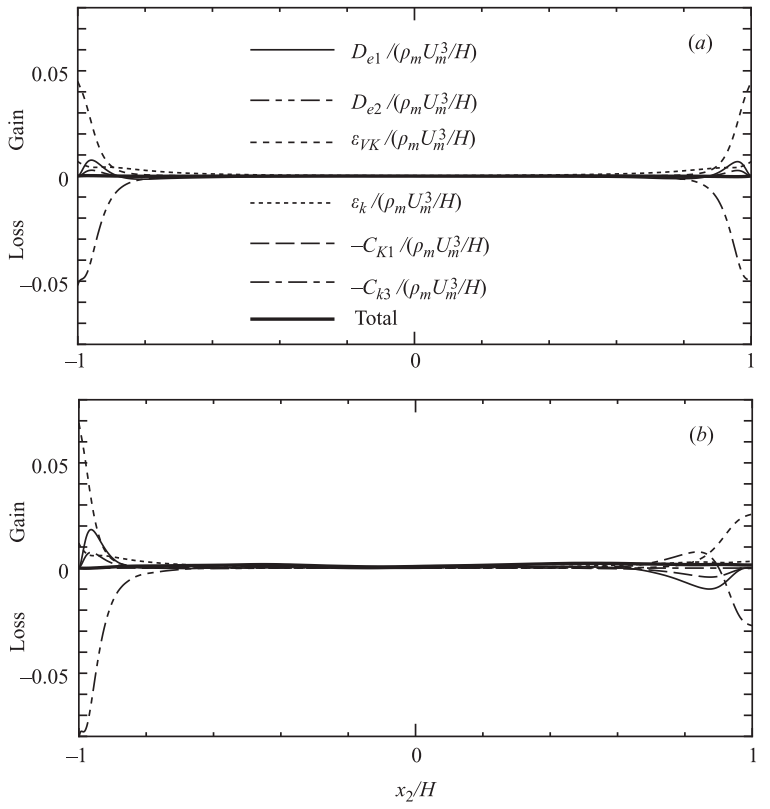

FIGURE 17. Internal energy budgets: (*a*) Case 1 and (*b*) Case 2.

does not exist in incompressible turbulent flow with passive scalar transport, because the viscous friction work does not appear in the energy (passive scalar) equation of incompressible turbulent flow (cf. (B 3) and (A 3)). For Cases A and B, artificial heat sources are added to the energy (passive scalar) equations instead of the viscous friction work, where the heat source of Case A is twice that of Case B (see (B 4)). As a result, the profiles of internal energy budgets of Cases 1 and 2 are different from those of Cases A and B. A qualitative comparison of the internal energy budgets between compressible and incompressible turbulent flows has no meaning, because their normalizations are different. Note that the peaks of turbulent and molecular diffusions do not appear near the adiabatic wall of Case B.

5.3. *Compressibility terms of turbulent and mean kinetic energy budgets*

The compressibility term of the turbulent kinetic energy equation, C_k, is almost zero and has a very small value in the region very close to the wall (see figure 14). On the other hand, the compressibility term of the mean kinetic energy equation, C_K, has a small value in the region very close to the wall (see figure 16). In the present simulations ($M = 1.5$), the result that C_k is almost zero is supported by the previous knowledge that the compressibility effect, like the pressure–dilatation correlation term, is negligible for wall-bounded compressible turbulent flow (e.g. Coleman *et al.* 1995; Huang *et al.* 1995; Guarini *et al.* 2000). Although some studies have been carried out to clarify the reason why the compressibility effect is small near the wall (e.g. Sarkar 1995; Friedrich & Bertolotti 1997), its detailed mechanism is still an open question.

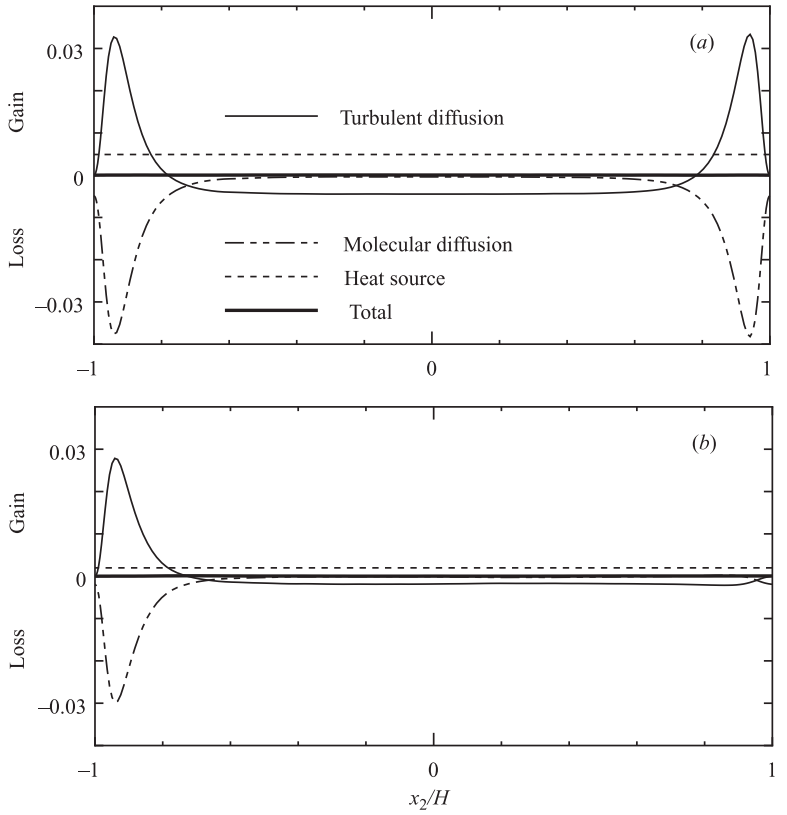

FIGURE 18. Budgets of passive scalar transport equation: (*a*) Case A and (*b*) Case B. The upper wall of Case B is adiabatic.

This is due to the lack of DNS data for quantitative investigation. Therefore, we first clarify the dominant terms in C_k and C_K. Then the roles of these terms with respect to energy transfers are investigated.

The compressibility terms in C_k are shown in figure 19. The pressure–dilatation correlation term C_{k3} (term 7 in figure 13) and the additional compressibility term C_{k1} (term 2 in figure 13) are almost zero near adiabatic and isothermal walls. The additional compressibility term C_{k2} (term 3 in figure 13) is dominant in C_k, and it has plus and minus values near isothermal and adiabatic walls, respectively. This implies that the term C_{k2} transfers turbulent kinetic energy to the mean flow near the isothermal wall and transfers energy from the mean flow to the turbulent flow near the adiabatic wall. This difference is explained as follows. The sign of C_{k2}, in which the term $\langle u_1'' \rangle \partial \langle \tau_{12} \rangle / \partial x_2$ is dominant, depends on that of $\langle u_1'' \rangle$, because $\partial \langle \tau_{12} \rangle / \partial x_2$ is always negative. The value of $\langle u_1'' \rangle$ is equal to $-\langle \rho' u_1' \rangle / \langle \rho \rangle$ (see (4.1)), which is positive and negative near isothermal and adiabatic walls, respectively. As a result, the value of C_{k2} is negative and positive near isothermal and adiabatic walls, respectively. Note that these energy transfers due to C_{k2} are small as mentioned above.

The compressibility terms in C_K are shown in figure 20. The term relating to the pressure work (term 5 in figure 13), C_{K1}, is dominant in C_K, and it has minus and plus values near isothermal and adiabatic walls, respectively. This means that the term C_{K1} exchanges internal energy for mean kinetic energy near the isothermal wall and exchanges mean kinetic energy for internal energy near the adiabatic wall. This

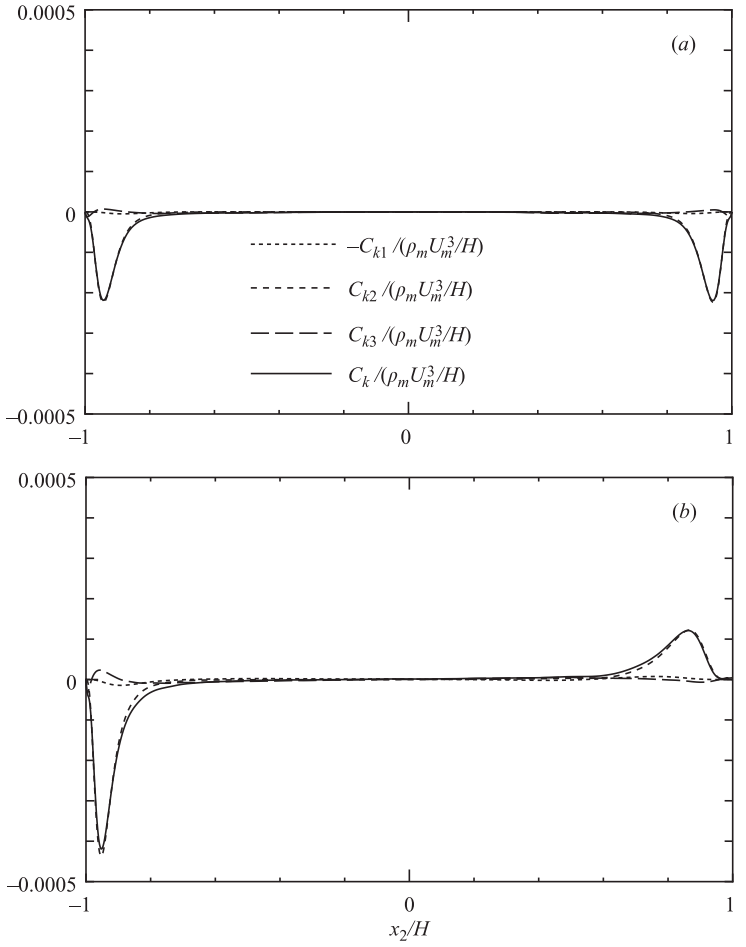

FIGURE 19. Compressibility terms of turbulent kinetic energy equation: (*a*) Case 1 and (*b*) Case 2.

difference can be explained by the result that the value of the mean dilatation $\langle d \rangle$ is positive and negative near adiabatic and isothermal walls, respectively (see Tamano 2002). Note that the negative and positive values represent the compression and expansion of the fluid, respectively.

5.4. *Dissipation terms of turbulent and mean kinetic energy budgets*

In this section, we consider the irreversible energy transfers due to the turbulent kinetic energy dissipation per unit volume ε_k and the mean kinetic energy dissipation per unit volume ε_{VK}. Using the vorticity fluctuation ω_i' and (5.5), ε_k is rewritten as.

$$\varepsilon_k = \langle\mu\rangle\langle\omega_i'\omega_i'\rangle - \frac{2}{3}\langle\mu\rangle\langle d'^2\rangle + \langle\mu'\omega_i'\omega_i'\rangle - \frac{2}{3}\langle\mu' d'^2\rangle + \frac{\partial\langle u_i\rangle}{\partial x_j}\left\langle\mu'\frac{\partial u_i'}{\partial x_j}\right\rangle + \frac{\partial\langle u_j\rangle}{\partial x_i}\left\langle\mu'\frac{\partial u_i'}{\partial x_j}\right\rangle - \frac{2}{3}\langle d\rangle\langle\mu' d'\rangle + 2\langle\mu\rangle\left\langle\frac{\partial u_i'}{\partial x_j}\frac{\partial u_j'}{\partial x_i}\right\rangle + 2\left\langle\mu'\frac{\partial u_i'}{\partial x_j}\frac{\partial u_j'}{\partial x_i}\right\rangle. \quad (5.9)$$

The enstrophy dissipation term $\varepsilon_{k1} = \langle\mu\rangle\langle\omega_i'\omega_i'\rangle$, the dilatational dissipation term $\varepsilon_{k2} = -(2/3)\langle\mu\rangle\langle d'^2\rangle$, the thermodynamic dissipation term $\varepsilon_{k3} = \partial\langle u_i\rangle/\partial x_j\langle\mu'\partial u_i'/\partial x_j\rangle$, and the total dissipation ε_k, are shown for Case 2 in figure 21. The value of ε_{k1} is

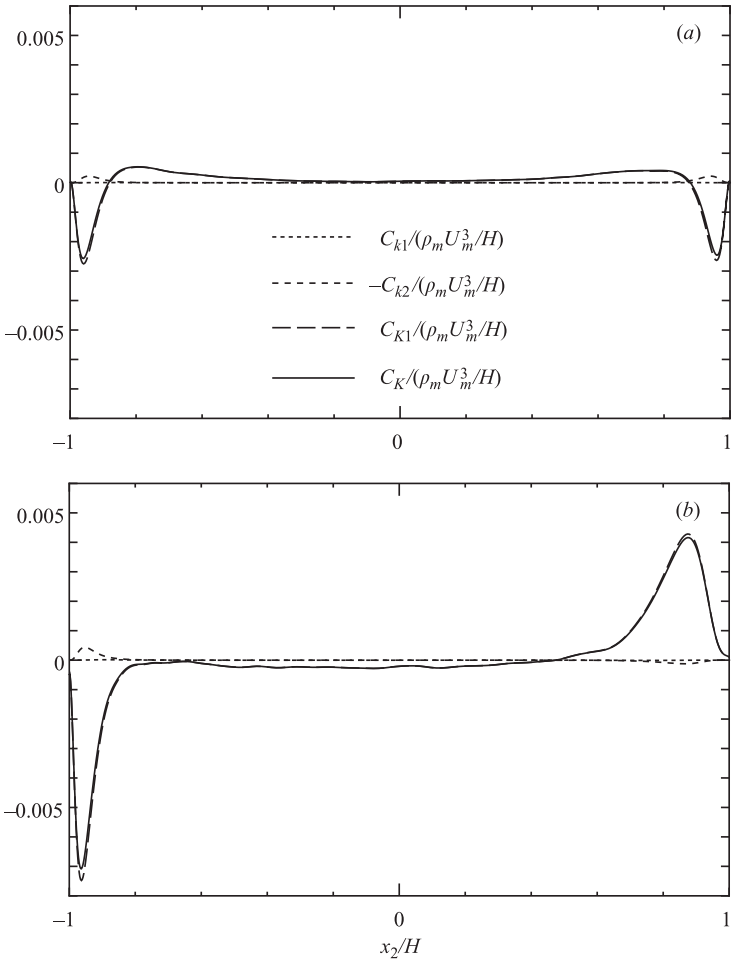

FIGURE 20. Compressibility terms of mean kinetic energy equation: (*a*) Case 1 and (*b*) Case 2.

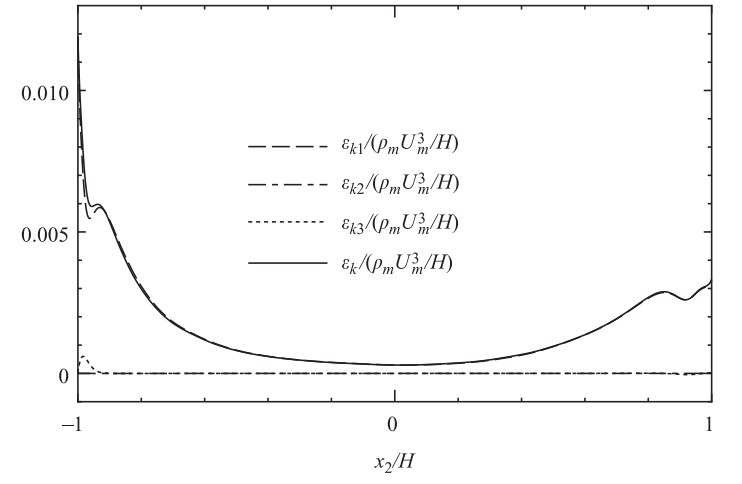

FIGURE 21. Turbulent kinetic energy dissipation per unit volume for Case 2.

dominant in the dissipation ε_k, and the value of ε_{k2} is almost zero. The ratio $\varepsilon_{k3}/\varepsilon_k$ is about 8% at $x_2/H = -0.98$ for Case 2, therefore ε_{k3} is not negligible in the region very close to the isothermal wall (see Huang 1995; Huang *et al.* 1995), while it is negligible near the adiabatic wall. We confirmed that the other terms of (5.9) were negligible. The sum of the second and the eighth terms on the right-hand side of (5.9) is the dilatational dissipation for homogenous compressible turbulent flow (see Sarkar *et al.* 1991).

Using the equation $\omega_i'\omega_i' = \partial u_i'/\partial x_j \partial u_i'/\partial x_j - \partial u_i'/\partial x_j \partial u_j'/\partial x_i$, equation (5.9) is rewritten as follows (see Huang 1995; Huang *et al.* 1995):

$$\varepsilon_k = \langle\mu\rangle \left\langle \frac{\partial u_i'}{\partial x_j}\frac{\partial u_i'}{\partial x_j} \right\rangle - \frac{2}{3}\langle\mu\rangle\langle d'^2\rangle + \left\langle \mu' \frac{\partial u_i'}{\partial x_j}\frac{\partial u_i'}{\partial x_j} \right\rangle - \frac{2}{3}\langle\mu' d'^2\rangle + \frac{\partial\langle u_i\rangle}{\partial x_j}\left\langle \mu' \frac{\partial u_i'}{\partial x_j} \right\rangle + \frac{\partial\langle u_j\rangle}{\partial x_i}\left\langle \mu' \frac{\partial u_i'}{\partial x_j} \right\rangle - \frac{2}{3}\langle d\rangle\langle\mu' d'\rangle + \langle\mu\rangle \left\langle \frac{\partial u_i'}{\partial x_j}\frac{\partial u_j'}{\partial x_i} \right\rangle + \left\langle \mu' \frac{\partial u_i'}{\partial x_j}\frac{\partial u_j'}{\partial x_i} \right\rangle. \quad (5.10)$$

The dissipation per unit mass, $\varepsilon_c = \varepsilon_k/\langle\rho\rangle$, is divided into the leading-order term which is the variable-density extension of the pseudo-dissipation used in the incompressible flow, $\varepsilon_{ci} = (\langle\mu\rangle/\langle\rho\rangle)\langle\partial u_i'/\partial x_j \partial u_i'/\partial x_j\rangle$, and the remainder which explicitly involves fluctuating dilatation or fluctuating viscosity, $\varepsilon_{cc} = \varepsilon_c - \varepsilon_{ci}$. Terms 6ic and 6c correspond to $\langle\rho\rangle\varepsilon_{ci}$ and $\langle\rho\rangle\varepsilon_{cc}$, respectively. The dissipations per unit mass, ε_{ci}^*, ε_{cc}^* and ε_c^*, which are normalized by $u_{\tau *}$, $\langle\rho\rangle$ and $\langle\mu\rangle$, are shown for Cases 2I and 2A in figure 22. The ratio $\varepsilon_{cc}^*/\varepsilon_c^*$ is about 11% at $y^* = 5.2$ for Case 2I, so that ε_{cc}^*, in which the main contribution is the thermodynamic dissipation term, is not negligible in the region very close to the isothermal wall, while it does not contribute near the adiabatic wall. Figure 22 also shows that the scaling with the local variables collapses the dissipation ε_c^* onto the data of the incompressible turbulent flow. We confirmed that the dissipation scaled by the wall variables did not agree well with the data of the incompressible turbulent flow.

We investigated the viscous dissipation per unit volume in the mean kinetic energy budget ε_{VK}, which was divided into the variable-density extended term of the pseudo-dissipation used in the incompressible flow (term 4ic in figure 13), $\varepsilon_{VKi} = \langle\mu\rangle(\partial\langle u_1\rangle/\partial x_2)^2$, and the remainder (term 4c in figure 13), $\varepsilon_{VKc} = \varepsilon_{VK} - \varepsilon_{VKi}$. We confirmed that the term ε_{VKc} was almost zero near adiabatic and isothermal walls for compressible turbulent flow (see Tamano 2002), therefore we ignore the energy transfer due to term 4c in figure 13.

5.5. *Energy transfers near adiabatic and isothermal walls*

The energy transfers near isothermal and adiabatic walls are summarized for compressible turbulent flow in figure 23. Term 1 is the energy transfer from the mean kinetic energy to the turbulent kinetic energy near adiabatic and isothermal walls in compressible turbulent flow. The roles of terms 2, 3, 5 and 7 with respect to compressibility are as follows (see § 5.3). Terms 2 and 7 do not contribute to energy transfers near isothermal and adiabatic walls. Term 3, which has a very small contribution to the energy transfer, transfers turbulent kinetic energy to the mean flow near the isothermal wall and transfers energy from the mean flow to the turbulent flow near the adiabatic wall. Term 5, which makes a small contribution to the energy transfer, exchanges internal energy for the mean kinetic energy near the isothermal wall and exchanges mean kinetic energy for the internal energy near the adiabatic wall. The roles of terms 4 and 6 with respect to dissipations, ε_{VK} and ε_k, are as follows (see § 5.4). Most of the energy transfers due to terms 4 and 6 are composed of the variable-density extended terms of the pseudo-dissipation used in the incompressible

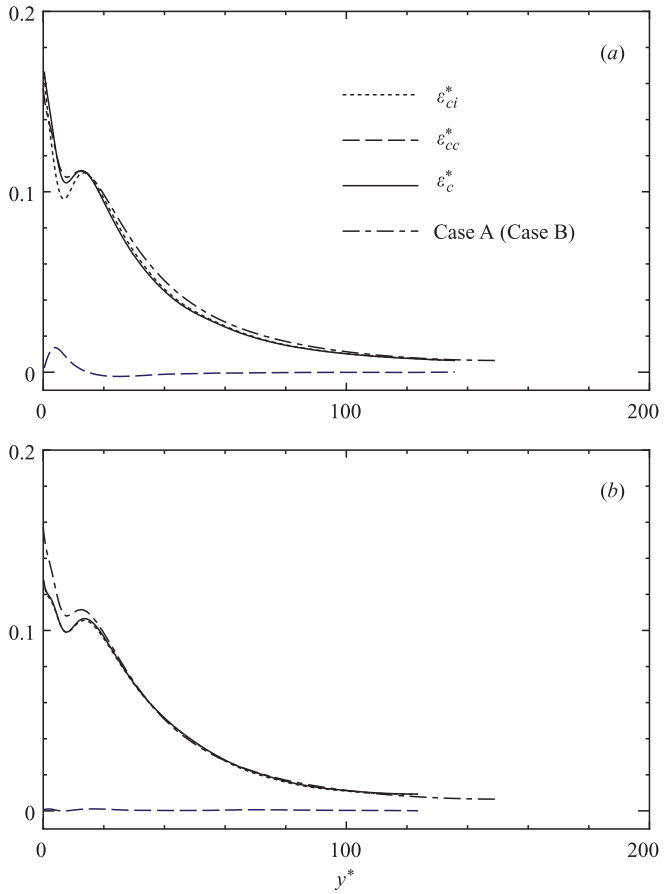

FIGURE 22. Turbulent kinetic energy dissipation per unit mass in semi-local wall units: (*a*) Case 2I and (*b*) Case 2A.

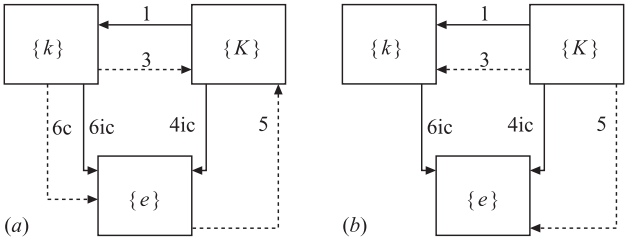

FIGURE 23. Non-negligible energy transfer of wall-bounded compressible turbulent flow: 1. P_k, 3. C_{k2}, 4ic. ε_{VKi}, 5. C_{K1}, 6c. $\langle\rho\rangle\varepsilon_{cc}$, 6ic. $\langle\rho\rangle\varepsilon_{ci}$, lines as figure 13, (*a*) near the isothermal wall (Case 1I or 2I) and (*b*) near the adiabatic wall (Case 2A).

flow (terms 4ic and 6ic). The term involving fluctuating dilatation or fluctuating viscosity (term 6c) is not negligible close to the isothermal wall.

For wall-bounded incompressible turbulent flows with passive scalar transport, the energy transfers due to terms 4ic and 6ic, which correspond to terms ε_{VK} and ε_k, do not exist, and only energy transfer in the due to term 1, which has the same role as in the compressible case, exists.

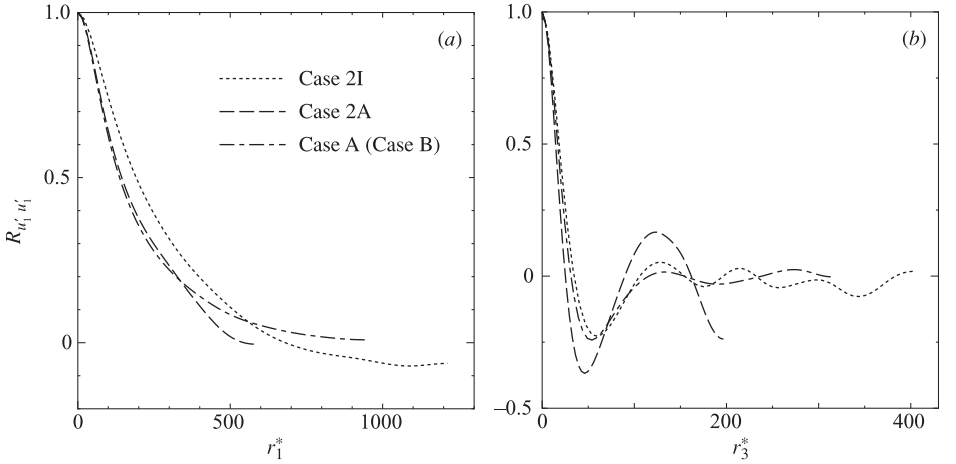

FIGURE 24. Two-point correlation of streamwise velocity fluctuation: (*a*) streamwise and (*b*) spanwise directions.

6. Near-wall turbulence structures

The streamwise and spanwise two-point correlations of streamwise velocity fluctuations, $R_{u_1'u_1'}(r_1^*)$ and $R_{u_1'u_1'}(r_3^*)$, are shown in figure 24, where $r_1^* = r_1/\delta_{v*}$ and $r_3^* = r_3/\delta_{v*}$ are the separations in the x_1- and x_3-directions, respectively. The two-point correlations of Cases 2I, 2A, and A are calculated at $y^* = 9.0$, 12, and 11, respectively. The streamwise two-point correlations for compressible turbulent flow go to zero within $L_1/(2\delta_{v*})$ and do not depend on the thermal wall boundary condition. It is found that the near-wall streaks of compressible turbulent flow do not become more coherent than those of incompressible flow. Hence, Morkovin's hypothesis is successful in the near-wall streak structures. This was also confirmed by the profiles of the skewness and flatness factors which are strongly related to the turbulence structure, in addition to the countours of the streamwise velocity fluctuation on (x_1, x_3)-planes (see Tamano & Morinishi 2002; Tamano 2002). Coleman *et al.* (1995) explained the modification of the streak using the ratio of turbulent and mean time scales used in the study of homogeneous turbulent shear flow by Lee, Kim & Moser (1990). However, we examined the profiles of the time-scale ratio and confirmed that there was no connection between the near-wall streak structures and the time-scale ratio. To clarify the relationship between the streamwise two-point correlation and the near-wall streak structure, more detailed examination in terms of the variations in the time and space may be required. We confirmed that the streamwise two-point correlations depended on the time and the wall-normal position for all cases in the present results. Smith & Metzler (1983) and Kim, Moin & Moser (1987) reported experimentally and numerically that the near-wall streaks had a mean spacing of about 100 in wall units and increased with this distance from the wall for wall-bounded incompressible turbulent flow. Figure 24(*b*) shows that the streak spacing of compressible turbulent flow is about 100 in semi-local wall units and is almost the same as for the incompressible case. The dependence of the near-wall streaks on the Mach number will be considered in future work.

Next, we investigate the correlation coefficient between streamwise velocity and temperature fluctuations, $R_{u_1'T'} = \langle u_1' T' \rangle / (\langle u_1'^2 \rangle^{1/2} \langle T'^2 \rangle^{1/2})$. Guarini *et al.* (2000) reported that the velocity–temperature correlations agreed well with the experimental

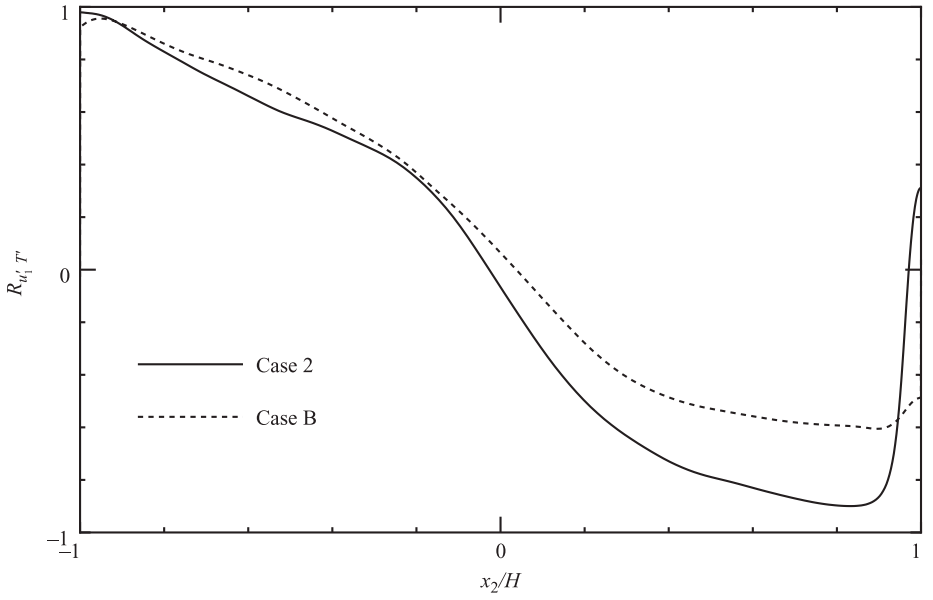

FIGURE 25. Correlation coefficients between u_1' and T' for Cases 2 and B.

and computational data on incompressible boundary layer flows because of weak compressibility. On the other hand, Nicoud (1999) reported that the peak value of the absolute velocity–temperature correlation near a heated wall was larger than that of a correlation near the cold wall and larger than that of Kim & Moin (1989) for incompressible turbulent flow. The correlations $R_{u_1'T'}$ are shown for Cases 2 and B in figure 25. The present results on the velocity–temperature correlation in the region very close to the isothermal wall are almost unity, $R_{u_1'T'} \simeq 1.0$, for both compressible and incompressible turbulent flows, and their profiles are almost the same. The peak value of the absolute correlation near the adiabatic wall of Case 2 is approximately 0.9, which is smaller than that near the isothermal wall. On the other hand, the correlation $|R_{u_1'T'}|$ near the adiabatic wall of Case B is approximately 0.5–0.6 and is smaller than that of Case 2. This is because the absolute values of temperature fluctuations near the adiabatic wall are very small for Case B. We confirmed that the production term in the equation of the temperature variance was almost zero near the adiabatic wall of Case B. The difference between Cases 2 and B near the adiabatic wall is not attributable to the variable property effect. In other words, Morkovin's hypothesis is not applicable to the correlation coefficient between velocity and temperature fluctuations near an adiabatic wall. We also examined the contours of the streamwise velocity and temperature fluctuations on (x_1, x_3)-planes, and confirmed that the low-speed streaks coincided with the low-temperature streaks near the isothermal wall and existed in the high-temperature regions near the adiabatic wall for compressible turbulent flow, while the corresponding relationship between streamwise velocity and temperature fluctuations was not observed near the adiabatic wall for the incompressible case (see Tamano & Morinishi 2002; Tamano 2002).

7. Conclusions

Direct numerical simulation of compressible turbulent channel flow between isothermal and adiabatic walls has been performed at Mach number $M = 1.5$ and

Reynolds number $Re = 3000$. A direct numerical simulation of incompressible turbulent channel flow with passive scalar transport between isothermal and adiabatic walls was also carried out for comparison. The main results are as follows.

The Van Driest transformed mean velocities near adiabatic and isothermal walls agree well with the data on incompressible turbulent flow. This can be explained by using the non-dimensional heat flux and the friction Mach number. The logarithmic region of the mean temperature near the isothermal wall does not appear for compressible turbulent flow because of the effect of the viscous friction work, while it appears near the isothermal wall in incompressible turbulent flow. And the difference of the mean temperature between compressible turbulent flows near isothermal and adiabatic walls is clarified.

The RMS temperature fluctuation profile scaled by the mean temperature is almost the same as that of the RMS density fluctuation profile scaled by the mean density, except that the RMS temperature fluctuation on the isothermal wall is zero. The wall-variable scaling does not result in such a similarity between temperature and density fluctuations. The difference between Favre and Reynolds averages on the Reynolds shear stresses is negligible. The semi-local scaling provides a universal profile of the Reynolds shear stress. On the other hand, the turbulent heat flux does not have a universal scaling in this study. The near-wall asymptotic behaviour of the wall-normal RMS velocity fluctuation for compressible turbulent flow is not equal to that of the incompressible case, even if the mean density variation is taken into account for the scaling. Thus, Morkovin's hypothesis is not applicable to near-wall asymptotic behaviour. The existing modified Reynolds analogies do not completely agree with the data on compressible turbulent flow for adiabatic and isothermal walls because of the influence of the opposite wall.

Although the compressibility term C_k of the turbulent kinetic energy equation has a slight contribution to the energy transfer, the dominant term of C_k transfers turbulent kinetic energy to the mean flow near the isothermal wall and transfers the energy of the mean flow to the turbulent flow near the adiabatic wall. This difference is due to the result that the correlation between the streamwise velocity and density fluctuations is positive and negative respectively near isothermal and adiabatic walls. The pressure–dilatation correlation term is almost zero near adiabatic and isothermal walls. The term relating to the pressure work is dominant in the compressibility term C_K of the mean kinetic energy equation. It exchanges internal energy for mean kinetic energy near the isothermal wall and also exchanges mean kinetic energy for internal energy near the adiabatic wall. This difference can be explained by the result that the value of the mean dilatation is positive and negative respectively near adiabatic and isothermal walls, where the negative and positive values represent the compression and expansion of the fluid, respectively. The thermodynamic dissipation term is negligible near the adiabatic wall, while it is not negligible in the region very close to the isothermal wall. On the other hand, the dilatational dissipation near adiabatic and isothermal walls is almost zero. The energy transfer due to the mean kinetic energy dissipation near adiabatic and isothermal walls in compressible turbulent flow is mainly composed of the the variable-density extended term of the pseudo-dissipation used in incompressible flow.

The two-point correlation of streamwise velocity fluctuations indicates that the near-wall streak structures of velocity for compressible and incompressible turbulent flows are comparable and independent of the thermal wall boundary condition, when the variable property effect is taken into account. Morkovin's hypothesis is thus successful for the near-wall streak structures. In addition, the correlation coefficient

between velocity and temperature fluctuations indicates that Morkovin's hypothesis is not applicable to the correlation coefficient between velocity and temperature fluctuations near the adiabatic wall.

The authors wish to thank Dr G. N. Coleman for providing the referenced data. The computations performed on a FUJITSU VPP300 at the Center for Promotion of Computational Science and Engineering, Japan Atomic Energy Research Institute, are gratefully acknowledged.

Appendix A. Governing equations for compressible flow

The continuity, momentum and energy equations are

$$\frac{\partial \rho}{\partial t} + \frac{\partial \rho u_j}{\partial x_j} = 0, \tag{A 1}$$

$$\frac{\partial \rho u_i}{\partial t} + \frac{\partial \rho u_i u_j}{\partial x_j} = -\frac{\partial p}{\partial x_i} + \frac{\partial \tau_{ij}}{\partial x_j} + \rho f_i, \tag{A 2}$$

$$\frac{\partial \rho T}{\partial t} + \frac{\partial \rho T u_j}{\partial x_j} = \frac{1}{c_v}\left[-p\frac{\partial u_j}{\partial x_j} + \tau_{ij}\frac{\partial u_i}{\partial x_j} - \frac{\partial q_j}{\partial x_j}\right], \tag{A 3}$$

where the viscous stress tensor $\tau_{ij} = \mu(\partial u_i/\partial x_j + \partial u_j/\partial x_i) - 2\mu\delta_{ij}\partial u_k/\partial x_k/3$ and the heat flux $q_j = -\kappa\partial T/\partial x_j$. The driving force f_i is given by

$$f_i = -\tau_{w_{av}}\delta_{i1}/(H\rho_m), \tag{A 4}$$

where $\tau_{w_{av}} = (\langle\tau_{12}\rangle_{x_1-x_3}|_{x_2=H} - \langle\tau_{12}\rangle_{x_1-x_3}|_{x_2=-H})/2$. Viscosity μ is given by Sutherland's law:

$$\frac{\mu}{\mu_{iw}} = \frac{1 + S_1/T_{iw}}{T/T_{iw} + S_1/T_{iw}}\left(\frac{T}{T_{iw}}\right)^{3/2}, \tag{A 5}$$

where S_1 is constant. The state equation is

$$p = c_p(\gamma - 1)\rho T/\gamma. \tag{A 6}$$

A mean pressure gradient is imposed to drive the flow in the DNS of incompressible turbulent channel flow. Although the driving force f_i has the same role in the DNS of compressible turbulent channel flow, it is not interpreted as the mean pressure gradient, since pressure is given by the state equation (A 6) (see Coleman *et al.* 1995; Huang *et al.* 1995).

Appendix B. Governing equations for incompressible flow

The continuity, Navier–Stokes and energy equations are

$$\frac{\partial u_j}{\partial x_j} = 0, \tag{B 1}$$

$$\frac{\partial u_i}{\partial t} + \frac{\partial u_i u_j}{\partial x_j} = -\frac{1}{\rho}\frac{\partial p}{\partial x_i} + \nu\frac{\partial^2 u_i}{\partial x_j \partial x_j}, \tag{B 2}$$

$$\frac{\partial T}{\partial t} + \frac{\partial T u_j}{\partial x_j} = \frac{\kappa}{\rho c_p}\frac{\partial^2 T}{\partial x_j \partial x_j} + Q. \tag{B 3}$$

The heat source Q is given by

$$Q = -q_{w_{av}}/(\rho c_p H), \tag{B 4}$$

where $q_{w_{av}} = (\langle q_2 \rangle|_{x_2=H} - \langle q_2 \rangle|_{x_2=-H})/2$.

REFERENCES

Antonia, R. A., Teitel, M., Kim, J. & Browne, L. W. 1992 Low-Reynolds-number effects in a fully developed turbulent channel flow. *J. Fluid Mech.* **236**, 579–605.

Bradshaw, P. 1977 Compressible turbulent shear layers. *Annu. Rev. Fluid Mech.* **9**, 33–54.

Coleman, G. N., Kim, J. & Moser, R. D. 1995 A numerical study of turbulent supersonic isothermal-wall channel flow. *J. Fluid Mech.* **305**, 159–183.

Dailey, L. D. & Pletcher, R. H. 1999 Large eddy simulation of constant heat flux turbulent channel flow with property variations. *AIAA Paper* 98-0791.

Fernholz, H. H. & Finley, P. J. 1977 A critical complication of compressible turbulent boundary layer data. *AGARD-AG* 223.

Fernholz, H. H. & Finley, P. J. 1980 A critical commentary on mean flow data for two-dimensional compressible turbulent boundary layers. *AGARD-AG* 253.

Friedrich, R. & Bertolotti, F. P. 1997 Compressibility effects due to turbulent fluctuations. *Appl. Sci. Res.* **57**, 165–194.

Gaviglio, J. 1987 Reynolds analogies and experimental study of heat transfer in the supersonic boundary layer. *Intl J. Heat Mass Transfer* **30**, 911–926.

Guarini, S. E., Moser, R. D., Shariff, K. & Wray, A. 2000 Direct numerical simulation of a supersonic turbulent boundary layer at Mach 2.5. *J. Fluid Mech.* **414**, 1–33.

Guo, Y. & Adams, N. A. 1995 Numerical investigation of supersonic turbulent boundary layers with high wall temperature. *Proc. 5th Summer Prog. 1994, NASA/Stanford Center for Turbulence Research*, pp. 245–267.

Horiuti, K. 1992 Assessment of two-equation models of turbulent passive-scalar diffusion in channel flow. *J. Fluid Mech.* **238**, 405–433.

Huang, P. G. 1995 Relations between viscous diffusion and dissipation of turbulent kinetic energy. Presented at the *10th Symp. on Turbulent Shear Flows, Penn. State U., August 14–16*, pp. 2-79–2-84.

Huang, P. G., Bradshaw, P. & Coakley, T. J. 1994 Turbulence models for compressible boundary layers. *AIAA J.* **32**, 735–740.

Huang, P. G. & Coleman, G. N. 1994 Van Driest transformation and compressible wall-bounded flows. *AIAA J.* **32**, 2110–2113.

Huang, P. G., Coleman, G. N. & Bradshaw, P. 1995 Compressible turbulent channel flows: DNS results and modelling. *J. Fluid Mech.* **305**, 185–218.

Kim, J. & Moin, P. 1989 Transport of passive scalars in a turbulent channel flow. *Turbulent Shear Flows 6*, pp. 85–96. Springer.

Kim, J., Moin, P. & Moser, R. 1987 Turbulence statistics in fully developed channel flow at low Reynolds number. *J. Fluid Mech.* **177**, 133–166.

Kleiser, L. & Schumann, U. 1980 Treatment of incompressibility and boundary conditions in 3-D numerical spectral simulations of plane channel flows. *Proc. 3rd GAMM Conf. on Numerical Methods in Fluid Mechanics* (ed. E. H. Hirschel), pp. 165–173. Vieweg, Brauschweig.

Lechner, R., Sesterhenn, J. & Friedrich, R. 2001 Turbulent supersonic channel flow. *J. Turbulence* **2**, 1–25.

Lee, M. J., Kim, J. & Moser, P. 1990 Structure of turbulence at high shear rate. *J. Fluid Mech.* **216**, 561–583.

Lele, K. 1994 Compressibility effects on turbulence. *Annu. Rev. Fluid Mech.* **26**, 211–254.

Maeder, T., Adams, N. A. & Kleiser, L. 2001 Direct simulation of turbulent supersonic boundary layers by an extended temporal approach. *J. Fluid Mech.* **429**, 187–216.

Morinishi, Y., Tamano, S. & Nakabayashi, K. 2003 A DNS algorithm using B-spline collocation method for compressible turbulent channel flow. *Computers Fluids* **32**, 751–776.

Morkovin, M. V. 1962 Effects of compressibility on turbulent flows. In *Mécanique de la Turbulence* (ed. A. Favre), pp. 367–380. CNRS.

Nicoud, F. C. 1999 Numerical study of a channel flow with variable properties. *CTR Annual Research Briefs 1998, Stanford Univ./NASA Ames*, pp. 289–310.

Robinson, S. K. 1991 Coherent motions in the turbulent boundary layer. *Annu. Rev. Fluid Mech.*, **23**, 601–639.

Rotta, J. C. 1960 Turbulent boundary layers with heat transfer in compressible flour. *AGARD Rep.* 281. NATO.

Rubesin, M. W. 1990 Extra compressibility terms for Favre-averaged two-equation models of inhomogeneous turbulent flows. *NASA Contractor Rep.* 177556.

Sarkar, S. 1995 The stabilizing effect of compressibility in turbulent shear flow. *J. Fluid Mech.* **282**, 163–186.

Sarkar, S., Erlebacher, G., Hussaini, M. Y. & Kreiss, H. O. 1991 The analysis and modelling of dilatational terms in compressible turbulence. *J. Fluid Mech.* **227**, 473–493.

Smith, C. R. & Metzler, S. P. 1983 The characteristics of low-speed streaks in the near-wall region of a turbulent boundary layer. *J. Fluid Mech.* **129**, 27–54.

Smits, A. J. & Dussauge, J. P. 1996 *Turbulent Shear Layers in Supersonic Flow*. American Institute of Physics.

So, R. M. C., Gatski, T. B. & Sommer, T. P. 1998 Morkovin hypothesis and the modeling of wall-bounded compressible turbulent flows. *AIAA J.* **36**, 1583–1592.

Spalding, D. B. 1961 On similarity solutions for free-convection flow past flat plates. *Trans. ASME: J. Appl. Mech.* **23**, 455–458.

Spina, E. F., Smits, A. J. & Robinson, S. K. 1994 The physics of supersonic turbulent boundary layers. *Annu. Rev. Fluid Mech.* **26**, 287–319.

Tamano, S. 2002 Direct numerical simulation of wall-bounded compressible turbulent flow. PhD thesis, Nagoya Institute of Technology.

Tamano, S. & Morinishi, Y. 2002 DNS of wall-bounded compressible turbulent flow. *Proc. 5th JSME–KSME Fluids Engng Conf., Nagoya, Japan, Novemver 17–21*, pp. 1461–1466 (CD-ROM).

Teitel, M. & Antonia, R. A. 1993 Heat transfer in fully developed turbulent channel flow: comparison between experiment and direct numerical simulations. *Intl J. Heat Mass Transfer* **36**, 1701–1706.

Van Driest, E. R. 1951 Turbulent boundary layer in compressible fluids. *J. Aero. Sci.* **18**, 145–160.

Wang, W. P. & Pletcher, R. H. 1996 On the large eddy simulation of a turbulent channel flow with significant heat transfer. *Phys. Fluids* **8**, 3354–3366.

Werne, J. 1995 Incompressibility and no-slip boundaries in the Chebyshev-tau approximation: Correction to Kleiserand Schumann's influence-matrix solution. *J. Comput. Phys.* **120**, 260–265

White, F. M. 1991 *Viscous Fluid Flow*, 2nd edn. McGraw-Hill.

Zhang, H. S., So, R. M. C., Speziale, C. G. & Lai, Y. G. 1993 Near-wall two-equation model for compressible turbulent flows. *AIAA J.* **31**, 196–199.